

Final Report

Force-Over-Area Engineering

Ezra Ameperosa

Rico Giovanni Ulep

Scott Miller

Kyle Seay



Project: Rimless Wheel Robot

Submission Date: 29 April 2015

In Partial fulfillment for the Requirements for Senior
Design 2 at the University of Texas at San Antonio

1. Abstract

Force Over Area Engineering has developed the Roadrunner Robot, a running robot which uses rimless wheels as its legs. The robot was designed to facilitate research on rimless wheels as a method of legged locomotion, with an emphasis on the cost of transport of rimless wheels in comparison to other common locomotion methods. As one of the simplest forms of legged locomotion, rimless wheels are ideal for application in rough terrain, as well as urban environments.

The robot uses a brushless DC motor to actuate its two rimless wheels and is designed for locomotion exceeding speeds comparable to human jogging speed (4 miles per hour). Real-time speed control is achieved through user input on a gamepad which is paired through radio frequency to a microcontroller inside the robot. The 8 spokes of each rimless wheel are made compliant by springs separating a pin-slot pair which compresses under the load of the robot. These compliant legs help reduce energy dissipation due to hard collisions with the ground and increase the Roadrunner Robot's running efficiency. The efficiency of the Roadrunner design was verified through a passive dynamic test, where it was proven to require less energy to achieve motion than a similar rigid-element robot. The Roadrunner Robot was also observed to achieve the desired speed of 4 miles per hour through a separate running test on a straight track, confirming that the design met the project's specifications.

Since the Roadrunner Robot is designed for research, versatility was a major priority for the design. Much of the Roadrunner Robot has been 3D printed using ABS Plus plastic, which allows rapid prototyping of additional parts and easy modifications of the existing design. This compatibility with rapid prototyping technology allows variables of the design (such as number of spokes or leg compliance) to be changed to collect a greater spectrum of data on rimless wheel legged locomotion.

Table of Contents

1. Abstract	i
2. Introduction and Background	1
2.1. Introduction	1
2.2. Background of Legged Motion	1
2.3. Background of Wheel Motion.....	2
2.4. Combining Legged and Wheel Motion - The Rimless Wheel	2
2.5. Statement of Problem.....	2
3. Purpose	3
3.1. Purpose	3
4. Objectives	3
4.1. Approach	3
4.2. Expected Accomplishments based on Research and Analysis.....	4
5. Engineering Design Specifications.....	5
5.1. Functional Requirements	5
5.2. Specifications	5
5.2.1.Dimensions	5
5.2.2.Weight	5
5.2.3.Motor	6
5.2.4.Number of Legs	6
5.2.5.Speed	6
5.2.6.Material	6
5.2.7.Microcontroller	6
5.3. Remote Control	6
6. Concept Designs	6

6.1.	Rigid Feet	7
6.2.	Spring Loaded Legs	8
6.3.	Prosthetic legs	9
6.4.	Pugh Decision Matrix for Choosing Final Design.....	10
7.	Final Design - Key Features and Analysis.....	10
8.	Fabrication	15
8.1.	3-D Printing	16
8.2.	Machining	18
8.3.	Ordered Parts	18
8.4.	Assembly	19
	8.4.1.Rimless Wheels	19
	8.4.2.Body	21
	8.4.3.Robot Assembly	21
9.	Testing	24
9.1.	Satisfying (functional) specifications	24
	9.1.1.Remote Control	24
	9.1.2.Speed	24
9.2.	Satisfying physical requirements	25
	9.2.1.Dimensions	25
	9.2.2.Weight	25
9.3.	Validation of Results	25
10.	Project Management	26
10.1.	Personnel	26
10.2.	Overall Schedule	27
10.3.	Personnel Assignments	27

10.4. Financial Performance	28
10.4.1.Overall Planned Cost vs. Time compared to Actual Cost vs. Time.....	28
11. Conclusions	29
12. Future Work	29
13. References	30
14. Appendix A.....	1
15. Appendix B.....	1

List of Equations

Equation A1: Mass Moment of Inertia of a Rod about the Central Axis (reference [8])	A1
Equation A2: Mass Moment of Inertia of a Rod about the End of the Rod (reference [8])	A1
Equation A3: Percent Change (reference [1]).....	A1
Equation A4: Passive Rimless Wheel Energy Loss after One step (reference [2])	A1
Equation A5: Rotational Energy (reference [9]).....	A1
Equation A6: Equation of Motion of Collision (references [10] & [11] & [4])	A2
Equation A7: Coefficient of Generation [3]	A2
Equation A8: Energy cost based on Coefficient of Generation [3]	A2
Equation A9: Energy Ratio of Passive and Springed Rimless Wheel [3]	A2
Equation A10: Coefficient of restitution of a spring damper system during collision [4]	A3
Equation A11: Bending Stress (reference [12]).....	A3
Equation A12: Axial Stress (reference [12]).....	A3
Equation A13: Shear Stress (reference [12])	A3
Equation A14: Endurance Strength (reference [12])	A4
Equation A15: Modified Goodman Fatigue (reference [12])	A4
Equation A16: Cycles to failure (reference [12])	A4
Equation A17: SLIP System Equation of Motion.....	A5

List of Tables

Table 1: Cost Analysis	27
Table A2: Mass Moment of Inertia Approximations	A6

<u>Table A3: Mass Approximations</u>	A7
<u>Table A4 Energy Loss</u>	A8
<u>Table A5: Remaining Energy per Mass</u>	A8
<u>Table A6: Energy Cost Comparison between Springed and Passive Rimless Wheel</u>	A9
<u>Table A7: Forces on Rod in phase</u>	A10
<u>Table A8 Forces on Rod out of phase</u>	A11
<u>Table A9 Force in Tube in phase</u>	A12
<u>Table A10 Force in Tube out of phase</u>	A13
<u>Table A11 Factor of Safety and Fatigue Cycles</u>	A14
<u>Table A12: Sizings</u>	A14
<u>Table A13: Operational Range Test Results</u>	A14
<u>Table A14: Pugh Chart Matrix</u>	A15
<u>Table A15: Speed Test Results</u>	A15
<u>Table A16: 3-D Part Dimension Test Results</u>	A16

List of Figures

<u>Figure 1: Rigid Feet Design</u>	7
<u>Figure 2: Spring Loaded Legs Design</u>	8
<u>Figure 3: Prosthetic Legs Design</u>	9
<u>Figure 4: Final Design Rendering</u>	10
<u>Figure 5: Spoke Assembly</u>	19
<u>Figure 6: Phase Arrangement</u>	19
<u>Figure 7: Roadrunner Assembly</u>	20
<u>Figure 8: Traceability Matrix</u>	22
<u>Figure 9: Senior Design 2 Schedule</u>	25
<u>Figure 10: Earned Value Chart (Based on Fully Loaded Industry Rates)</u>	26
<u>Figure A11: Expected 3-D Part Dimensions</u>	A16
<u>Figure A12: Approximate Shape</u>	A17
<u>Figure A13: Cost Effectiveness of Spoke Configurations</u>	A17

<u>Figure A14: Free Body Diagram of design</u>	A18
<u>Figure A15: Exploded Leg assembly</u>	A19
<u>Figure A16: Spring Loaded Inverted Pendulum (SLIP) System</u>	A19
<u>Figure A17: Case Layout</u>	A20
<u>Figure A18: Robot In-Phase and Anti-Phase</u>	A21
<u>Figure A19: Deflection of Spring at 4 MPH</u>	A22
<u>Figure A20: Bearing Test Fixture</u>	A22
<u>Figure B21: Leg Assembly</u>	B1
<u>Figure B22: Spoke Assembly</u>	B2
<u>Figure B23: Body Assembly</u>	B3
<u>Figure B24: Motor Assembly</u>	B4
<u>Figure B25: Microcontroller Assembly</u>	B5
<u>Figure B26: Axle</u>	B6
<u>Figure B27: Tube</u>	B7
<u>Figure B28: Rod</u>	B8
<u>Figure B29: Flange</u>	B9
<u>Figure B30: Hub</u>	B10
<u>Figure B31: Case Lid</u>	B11
<u>Figure B32: Case 1</u>	B12
<u>Figure B33 Case 2</u>	B13
<u>Figure B34: Case 3</u>	B14
<u>Figure B35: Case 4</u>	B15
<u>Figure B36: Motor Plate 1</u>	B16
<u>Figure B37: Motor Plate 2</u>	B17
<u>Figure B38: Spur Gear</u>	B18

Symbols, Units, and Acronyms

UTSA – University of Texas at San Antonio
RAM Laboratory – Robotics and Motions Laboratory
FOA – Force Over Area Engineering
3D – Three Dimensional
FDM – Fused Deposition Modeling
DC – Direct Current Motor
BLDC – Brushless Direct Current Motor
ESC – Electronic Speed Control
LiPo – Lithium Polymer Battery
MPH – Miles Per Hour
ABS – Acrylonitrile butadiene styrene (3D printing plastic)
MATLAB – Matrix Laboratory software
RPM – Revolutions per minute
CPI – Cost Production Index
SPI – Schedule Production Index
CSI – Cost Schedule Index
BCWP – Budgeted Cost of Work Performed
ACWP – Actual Cost of Work Performed
BCWS – Budgeted Cost of Work Scheduled
CAD – Computer-aided Design Software
SolidWorks – Computer-aided 3D Modeling Design Software
SLIP – Spring Load Inverted Pendulum

2. Introduction and Background

2.1. Introduction

For mechanical locomotion in robotics, wheels are typically favored due to the efficiency and tipping stability that is inherent in their geometry. Legged locomotion is an alternative to wheeled motion, but typically involves lifting, repositioning, and planting a leg, all of which consume energy for a relatively small distance traveled. Wheeled motion is much less complex, doesn't dissipate energy through inefficient pathing like a legged 'step,' and is not exposed to hard collision impact forces against the ground. The geometry of wheels simplifies the tipping stability of the wheel because the wheel cannot 'fall' in the direction of travel, as that would simply cause the wheel to roll. However, wheels can be undesirable on rough terrain, where wheeled locomotion may not be possible and may cause damage to the robot. To improve on this problem, some robot designs emulate the locomotion of humans and animals, which are more capable of operating on rough or uncertain terrain because of their legged movement. However, humanoid biped robots require complex algorithms and control systems to maintain balance. Additionally, biped locomotion is typically inefficient and slow due to the complexity of the control systems and the precision required for these controls. Thus, there is a need in robotics for a solution that combines the benefits of the wheel and legged locomotion to produce a reliable and efficient mode of transportation on rough terrain.

2.2. Background of Legged Motion

Legged locomotion in robotics is a difficult problem involving complex path generation computations and control systems. Modern humanoid legged robots, such as Honda's state-of-the-art biped, Asimo, have sophisticated control systems which allow it to balance itself when standing on flat ground and shuffle its feet to travel short distances. However, these control systems do not adapt based on the environment or react to obstacles.

The major source of inefficiency in legged locomotion comes from the dissipation of energy in every step through impact forces. Impact forces are the forces experienced by the foot of the robot as it comes into contact with the ground, similar to forces experienced in human locomotion. In rigid body running, these forces cause dissipation of energy from the rigid body

to the ground, effectively losing energy from the system which must be replaced through a power source for sustained locomotion to continue. However, human dynamics presents a solution to this, as the muscles and tendons in human legs act as linear springs to allow energy absorption to soften the effects of impact forces. By translating some of this impact into potential energy through the 'leg spring,' humans are able to reduce the energy lost to the ground through hard collisions.

2.3. Background of Wheel Motion

Wheeled locomotion is typically the favored method of locomotion in robotics for smooth, flat terrain. The simplicity and efficiency of the wheel contribute to the reliability of these robots, but wheeled locomotion has a fatal flaw: wheels cannot operate on rough or uncertain terrains and perform poorly on slopes. Thus, though wheeled locomotion is simple and energy-efficient, the applications of such technology are extremely limited.

2.4. Combining Legged and Wheel Motion - The Rimless Wheel

One model that combines the benefits of wheeled motion and legged locomotion is called a rimless wheel. The rimless wheel is considered to be the simplest and most efficient legged walking model. This model consists of a central hub with several spokes extending radially from the hub in a symmetric pattern. The number of spokes on the rimless wheel greatly affects its dynamic characteristics; adding spokes better approximates the energy-efficiency of a wheel, but adds weight to the assembly and reintroduces the shortcomings of the rimmed wheel. Though the rimless wheel borrows many successes of rimmed wheels, rimless wheels are not as efficient as wheels on smooth terrain due to the hard collision impact forces that the legged locomotion rimless wheels encounter.

2.5. Statement of Problem

Most common methods of legged locomotion are impractical for most applications on smooth terrain due to excessive energy loss to hard collisions. For most legged robots, the cost of transport is prohibitively high and such legged robots are often ignored in favor of more efficient

options, most commonly wheels. However, wheels are not viable options in rough or uncertain environments, which leads to a lack of energy-efficient locomotion methods for rough terrain.

3. Purpose

3.1. Purpose

The purpose of the Roadrunner project is to develop a legged robot that achieves locomotion on level ground using a rimless wheel design.

4. Objectives

The objective of the Roadrunner project is to develop a legged running robot capable of achieving speeds comparable to human jogging speed (4 MPH).

4.1. Approach

To approach this design problem, Force Over Area first conducted research on rimless wheels to understand the dynamics of their motion and how they model humanoid walking. Several journals and scholarly articles on the subject of non-actuated rimless wheels, called passive rimless wheels, were found and investigated. Passive dynamic testing of the rimless wheel can be conducted by placing a non-actuated rimless wheel on a slanted smooth surface at a set slope to model its energy characteristics, which are obtained from the object's potential energy at a measured height on the slope. However, research papers discussing rimless wheel motion on a zero slope were sparse, suggesting a lack of data on the subject and a need for experimental data for a rimless wheel which operates on flat terrain. Because the rimless wheel is a method of legged locomotion despite its physical similarity with a wheel, it must supply enough energy to make up for the energy it dissipates to the ground with every step through hard collisions. This challenge is what makes legged locomotion generally not preferred compared to the much more ubiquitous wheeled locomotion; therefore, our robot seeks to improve on this weakness to produce an energy-efficient method of legged locomotion using rimless wheels.

With the knowledge gained through this research and the observations of collected data, the team was able to begin drafting solutions to the energy problems which make legged locomotion

undesirable, with the goal of achieving locomotion on a flat plane (as opposed to a negative slope, where gravity helps pay the cost of transport). The team created three unique concept designs which each used distinct approaches to design a rimless wheel capable of locomotion on a flat plane. Analysis was conducted on the concept designs produced by the team, to verify an improvement over rigid rimless wheels and justify the design decisions. A single design was chosen using a Pugh decision matrix to objectively evaluate the concept designs. Detailed analysis of the chosen design was conducted to determine the material and dimensions characteristics that would be required for the design to be functional.

The rimless wheels of the Roadrunner Robot are made by 3D printing using Fused Deposition Modeling (FDM) of ABS plastic material. This design approach allows rapid prototyping of the design and facilitates easy replacement of parts. Additionally, 3D printing allows versatility in the robot so that the number of spokes on the rimless wheel can be modified, custom end-effectors for the spokes may be added, and dimensions may be tuned. Several test 3D prints were conducted to evaluate the printing resolution which could reasonably be expected.

Fabrication progressed through a few iterations and the final assembly was constructed with the 3D printed parts, 4 unique machined aluminum and steel parts, and several purchased electronics including a motor and a microcontroller. The motor is controlled through an Electronic Speed Control (ESC) which receives signal inputs from a remote control through an Arduino Mega 2560 microcontroller. The final Roadrunner Robot is composed of many modular subassemblies which can be independently replaced or modified without changing its mates.

Finally, the Roadrunner Robot was tested to verify that the project had met the outlined specifications. The main tests focused on the robot's linear velocity and a passive dynamic test which sought to prove that the Roadrunner Robot has improved efficiency compared to a similar rigid robot.

4.2. Expected Accomplishments based on Research and Analysis

Research related to the dynamics of a mass-spring-damper system and running motions of human legs (modeled as spring-dampers) suggested that the springs in the robot would diminish the energy lost to hard collisions, and reduce the amount of energy required to power the system.

The Roadrunner Robot was compared to a similar rigid-spoke rimless wheel robot and was confirmed to require less energy to move. The team experimentally validated that the Roadrunner Robot was capable of locomotion on flat terrain at the desired velocity (4 MPH).

5. Engineering Design Specifications

The design of this robot must accomplish several functional and physical requirements and specifications. The specifications are defined by the expected requirements the robot will need to operate as requested by the project's sponsor, Dr. Pranav Bhounsule.

5.1. Functional Requirements

The project's main goal is to achieve locomotion, so the main functional requirement will be to achieve and sustain a speed of 4 miles per hour. Another important requirement is cost-efficiency, so the prototype will be tested and compared to a rigid rimless wheel to verify that the design improves on a rigid body rimless wheel.

5.2. Specifications

The project sponsor and mentor, Dr. Pranav, outlined several specifications so the prototype robot will fit his research needs for the Robotics and Motions Laboratory.

5.2.1. Dimensions

The robot must be a size and weight that allows it to be easily transported to different sites for testing and demonstration. The robot dimensions must not exceed 2 feet in height and 1.5 feet in width.

5.2.2. Weight

An average human adult should be capable of easily transporting the robot. The robot's weight must not exceed 15 lbs.

5.2.3.Motor

The minimum speed the Roadrunner must achieve is 4 mph (1.8 m/s). To achieve this specification, the motor that has been chosen is a DC brushless motor that has a continuous torque rating of 15 in-lbs.

5.2.4.Number of Legs

The number of spokes affects the energy loss and stability of the rimless wheel. The robot design must have no fewer than 3 spokes per wheel, and no more than 12 spokes per wheel.

5.2.5.Speed

The robot should move at a minimum speed of around human jogging speed. The robot must operate a minimum speed of 4 miles per hour.

5.2.6.Material

The material properties must be sufficient for the expected loads from impact while the robot is in operation.

5.2.7.Microcontroller

A microcontroller will be used to receive commands from the robot operator through radio frequency, and output speed and controls commands to the motor through the ESC.

5.3. Remote Control

The remote control must communicate with the robot from a distance exceeding 50 feet. The remote control must have sufficient capabilities for a minimum of 3 inputs: stop motor, increase motor speed, decrease motor speed.

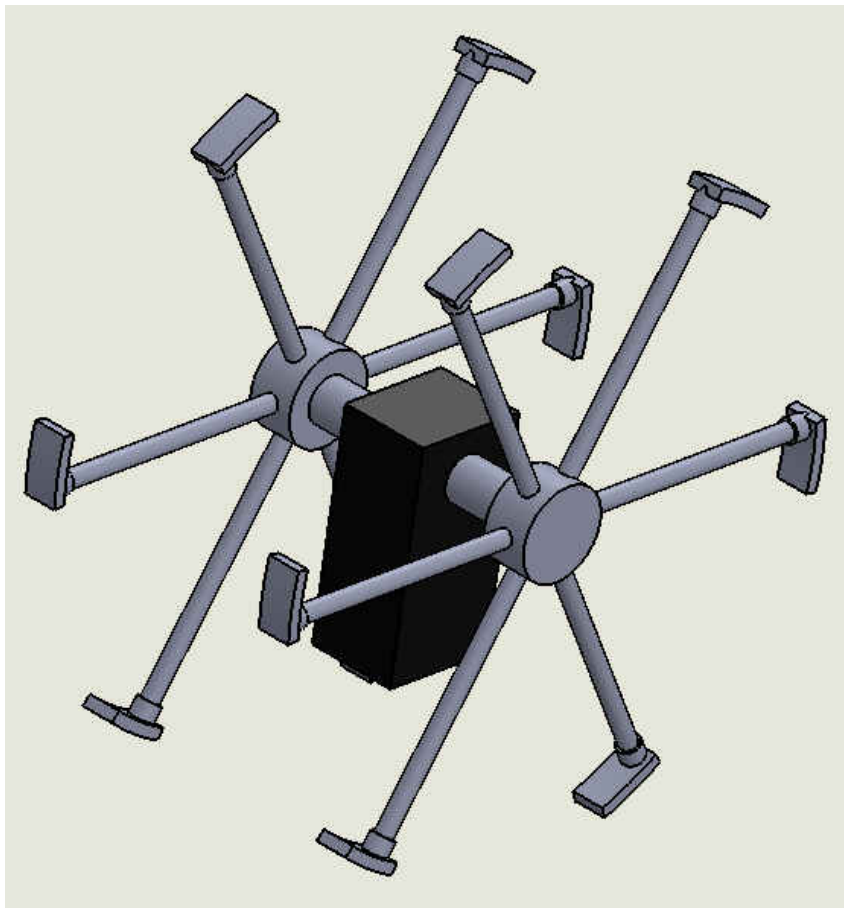
6. Concept Designs

Several concept designs were initially drafted and analyzed based on cost, manufacturability, and expected performance. These concept designs were compared using a Pugh Decision-Matrix analysis method to objectively choose the best concept design. The designs have a central torso which houses the electrical components and protects them from the environment and from potential damage from impacting obstacles. This torso will be constructed from ABS 3D printing

plastic, which was found to have sufficient stress characteristics to support the required loads. The benefit of using ABS plastic over other considered materials is that 3D printed components can be quickly and economically replaced or modified. ABS plastics have less desirable material properties than the second material choice, Aluminum, but are also lighter, which reduces weight and therefore the importance of the material properties. Another advantage is that ABS plastic allows for much greater design flexibility, which opens many possibilities for variable data collection from this robot.

6.1. Rigid Feet

This concept design improves on the typical passive rimless wheel by reducing the effective step angle of the robot, which decreases the effects of hard collisions on the energy dissipation of the robot. This is accomplished by spokes which have end effectors resembling human feet. These



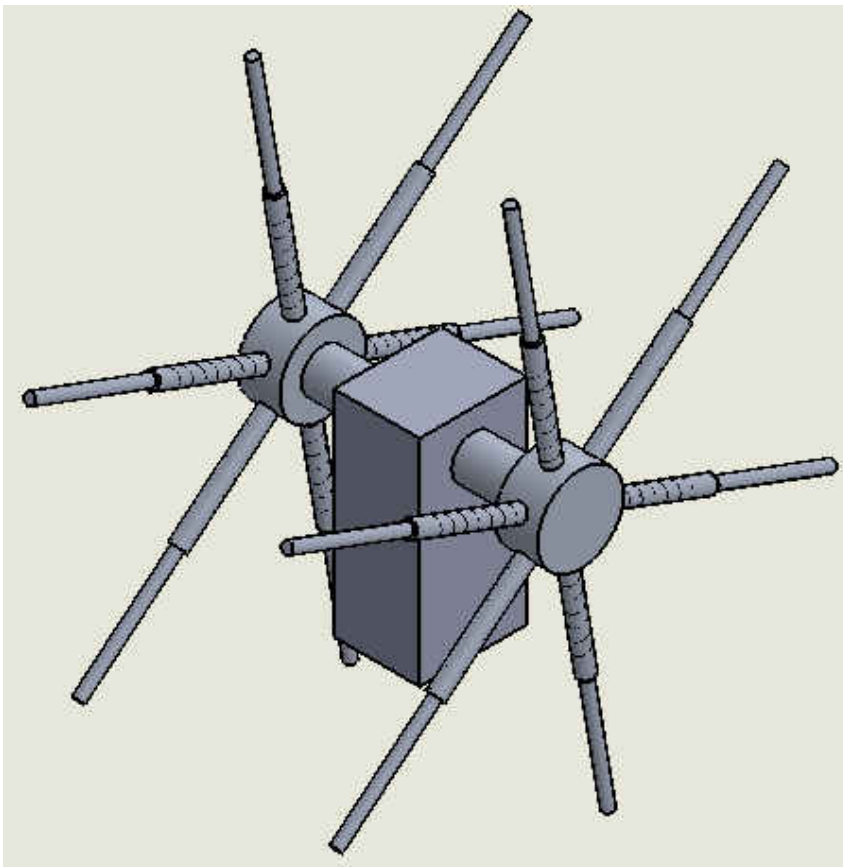
feet are asymmetric, forming a “heel” and “toe” to the robot foot. The feet will be flexed to approximate the radius of curvature of a rimmed wheel of similar dimensions. This will introduce some of the benefits of wheeled motion, and apply them to the legged robot design. The energy loss per step will be decreased because of the shorter step angle (from toe of the supporting spoke to the heel of the next spoke). The

friction forces experienced by the robot will increase due to the curved feet mimicking wheeled

motion behavior, however friction forces are much less destructive than hard collisions in the case of legged locomotion, so a net energy gain is experienced. This design better approximates wheeled motion, and therefore reduces the robot's ability to navigate "rough" terrain. The scope of this project defines rough terrain to be changes in terrain height that are not trivially small (e.g. 1/50 of radius of curvature). Additionally, this design suffers because there are no considerations for damping the hard collision forces experienced, which causes greater stress to the members, and also dissipates energy into the ground at a greater rate than damped spokes.

6.2. Spring Loaded Legs

The spring loaded design takes advantage of spring kinematics to reduce the amount of energy lost to hard collisions. The spring loaded legs are constructed by having one end of a tube



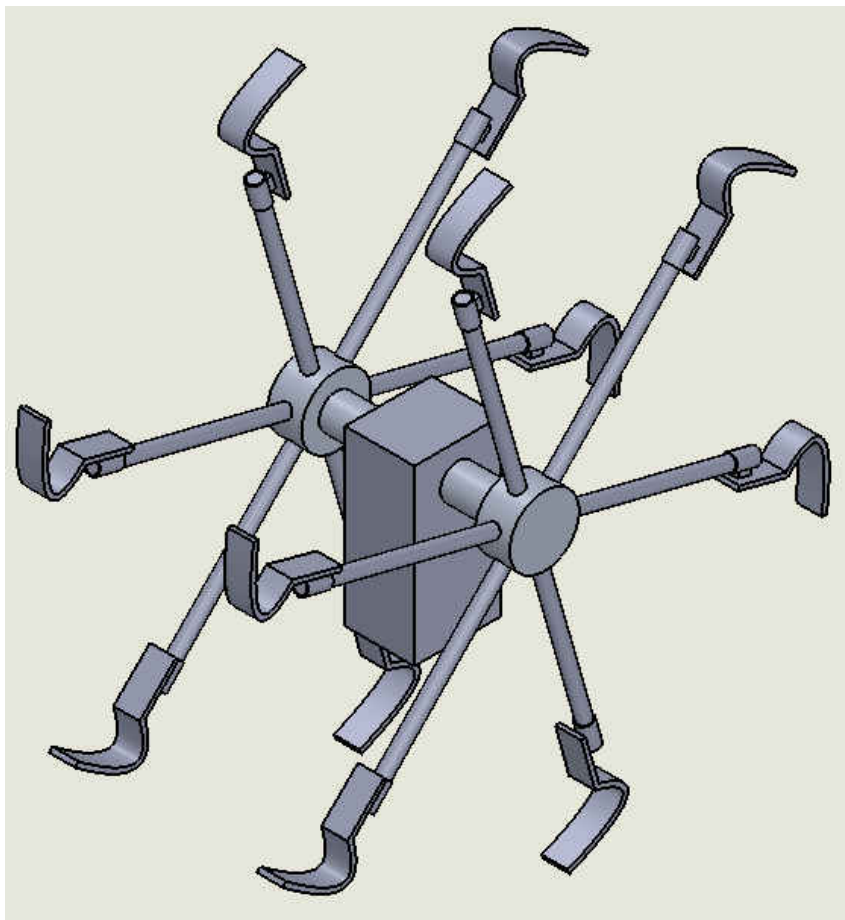
connected to the hub. The other end of the tube has a rod that slides within the tube with a spring connected to both the rod and tube. The rod has a slot at the end that slips in and out of the tube and is connected to the tube by a pin to restrict the rod from escaping the tube. As the robot steps, the spring within the supporting spoke depresses, storing energy in the form of potential energy, until the load from

the weight of the robot is directly above the supporting spoke. At this point, the spring is at its

fully compressed state and begins to release its stored energy as kinetic energy as it passes the fully compressed state, extending the legs out, pushing the robot forward. With this design, the spokes dampen the collision of hitting the ground and help improve the energy-efficiency of the design.

6.3. Prosthetic legs

The prosthetic leg design draws its inspiration from a type of prosthetic which uses curved spring steel to simulate the spring characteristics of leg muscles. The type of prosthetic leg we analyzed



and adapted for this design was an active carbon fiber prosthetic used for running applications. The prosthetic leg design is a combination of the rigid foot and the spring loaded leg designs, as the design has feet extending from the spoke while also providing a spring effect due to the geometry and the material of the leg. The prosthetic leg has proven to be a feasible design for high speed locomotion by Oscar Pistorius, a double amputee runner who used prosthetic

legs to compete in the 100 and 200 meter race in the Paralympics earning him a medal for both. Oscar Pistorius' accomplishments using prosthetic legs serve as a proof of concept for using the

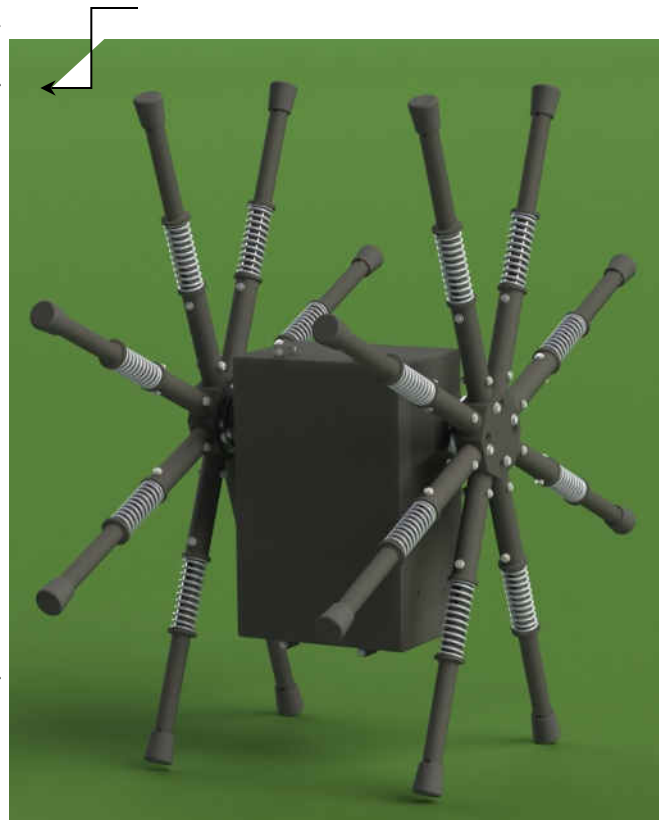
prosthetic leg design for the running robot to support its weight and provide spring-like characteristics of leg muscles.

6.4. Pugh Decision Matrix for Choosing Final Design

The concept designs were initially drafted and analyzed based on cost, manufacturability, and expected performance. These concept designs were compared using a Pugh Decision-Matrix analysis method to objectively choose the best concept design (Table A14). The Pugh Decision Matrix clearly shows that the Spring Loaded Legs design is the best design of the three, so the team chose this design to develop into a final design (Figure 2).

7. Final Design - Key Features and Analysis

The spring loaded design takes advantage of spring kinematics to reduce the amount of energy lost to hard collisions. The slot and pin design of the spokes restrict the rod from escaping the tube (Figure A15). The flange design allows for in-phase, anti-phase, or variable phase leg configurations (Figure A18). It includes a central torso which houses the electrical components and protects them from dust, dirt, and from potential damage from impacting obstacles (Figure A17). It utilizes a Brushless DC Motor to propel itself forward in conjunction with an Electronic Speed Controller. Finally, it can be remote controlled using radio frequency transmission.



The methods used to build and evaluate this design include: research and numerical analysis of passive (non-powered) rimless wheels, dynamic analysis of a passive rimless wheel with varying number of spokes, analysis on spring deflection, research and numerical analysis of energy dissipation in plastic and springed collisions, stress approximations for the spokes, and an analysis on the motor specs required to propel the design forward.

Most of the published material on the dynamics of passive rimless wheels were found to be theoretical, and thus each neglected different variables to simplify their theoretical analysis. Thus, the assumptions made in these papers had to be thoroughly analyzed by FOA, and the equations modified to fit the project at hand. In the published material about the analysis of physical rimless wheel assemblies, several departures from our own design were made by each of the robots, and therefore the experimental results could not be blindly applied to our design. The combined research of rimless wheels yielded several educated predictions of how the design can be expected to perform.

The number of spokes on a rimless wheel determines the behavior of the rimless wheel, with behavior approximating that of a wheel when the number of spokes is arbitrarily large. Since each spoke would increase costs associated with cost of transport due to weight and cost of materials, it was necessary to find a configuration which was suitable in terms of performance and cost.

To obtain this suitable number of spokes, an analysis was done on the energy lost after each step of the rimless wheel. To achieve this, an approximation of the mass moment of inertia for the design must be obtained. Equation A1 and Equation A2 were used to accomplish this. Assuming that each cylinder had a radius 0.5 in., had a density of 0.0376 lbm/in³, and was 12 in. long, the mass moment of inertia of a rod from the central axis and at the end of the rod were found to be 0.0443 lbm* in³ and 17.032 lbm*in³. These values were then be used to approximate the mass moment of inertia of the basis of a rimless wheel design about its center with different spokes per side. These values are shown in Table A2. The mass of the design was also approximated in

, and each spoke is 0.3544 lbm. An example of a 4 spoke configuration is shown in Figure A12.

Using these values for the mass moment of inertia at different numbers of spokes and assuming an initial angular velocity before each collision/step of 9 rad/s, Equation A4 was used to find the angular velocity after each collision/step. These values are shown in Table A4 Energy Loss. Table A4 also shows the rotational energy before and after the collision using Equation A5. For ease, these values were generated using MATLAB.

Increasing the number of spokes increases the energy-efficiency of the rimless wheel, however the additional mass and cost added by these spokes creates a diminishing returns effect. Thus, the number of spokes on the rimless wheel subassembly must be optimized such that the rimless wheel benefits in terms of energy-efficiency from having many spokes, but also avoids having too many spokes which would decrease the energy-efficiency through added weight. Table A5 is an extension of Table A4 and shows the percentage of energy that remains after each collision. It also shows the ratio of the energy remaining to the mass of the configuration. This ratio is significant because the higher the ratio of energy remaining to the mass, the more cost effective the design, therefore it is favorable to choose the configuration that produces the highest ratio.

Figure A13 illustrates this data graphically and shows that as you increase the number of spokes there is a peak where the design will be the most cost effective. It is seen that 8 or 9 spokes per side is the best number of spokes to create the most cost effective design. 8 spokes was chosen due to the simple angles and the symmetry it provides making further analysis more manageable.

Due to the slot and pin design, the maximum allowable deflection of the spring leg is 1.5 inches. Larger values will cause collisions between the pin and the slot to occur in the legs which is undesirable and inefficient. Therefore, an analysis of the expected deflection of the springs and the spring rates must be executed.

Research in the subject reveals a model of a spring loaded inverted pendulum (SLIP) system (Figure A16). This model is widely known in the field of robotics and has been examined many times [15]. After finding equations of motion for such a system (Equation A17), MATLAB was used to find the deflection of a robot of weighing 10 pounds with a leg length of 12 inches.

Figure A19 illustrates that as the spring rate is increased, the deflection decreases. It also shows that the minimum spring rate the robot must have is about 13 lb/in. Based on availability, a spring rate of 17.5 lb/in was chosen as it allows for a lesser deflection than allowed and provides adequate leeway in the case that more deflection occurs, which will happen at velocities higher than the design speed.

The hard collisions experienced by passive rimless wheels cause energy to be dissipated to the ground at each of these collisions. These collisions are to be considered are plastic collisions, which means all energy is absorbed during the impact. Our design deals with springs, so the task is to model the collisions in a springed system.

To accomplish this, the behavior of our springed system with respect to gravity alone is described in Equation A6. Using MATLAB, this equation was solved for the first non-trivial solution of x at different initial velocities. These times represent the amount of time it takes for a collision to occur. Using MATLAB, these times were used to find the velocity after a collision, which is then used with Equation A10 to find the coefficient of restitution for the collisions at different speeds. The coefficient of restitution is the ratio of speed after and before an impact. This was converted to the coefficient of generation, e_g , using Equation A7. The reason for this is to avoid case where the coefficient of restitution, e_r , is infinite [3] (Table A6).

For passive rimless wheels the collisions are plastic, so e_r is equal to 0 and e_g is equal to -1. Equation A8 introduces a new variable which is the elastic recovery, r , which is ratio of the amount of energy that is recovered from the collision. In this analysis it is assumed to be 0, meaning that all energy that is absorbed in the collision must be replaced by the motor. This

assumption is made such that the amount of energy needed from the motor can be more safely approximated. Using Equation A8, the ratio of energy costs of a passive rimless wheel and a springed rimless wheel was found for different speeds. Since some parameters are the same for both, all that's left of the equation after the ratio will equate to Equation A9. This data is shown in Table A6 and shows that a springed collision has 30-40% of the energetic cost of a plastic collision and that this efficiency increases as the speed of the collisions increase.

Stress calculations for the design were necessary so that it does not fail during operation. To accomplish this, the forces that the robot will be subjected to must be approximated. Looking into some research on the forces involved in human running based on the body weight of the person, it can be approximated that the maximum amount of force the robot will experience vertically and horizontally is 3 and 0.5 times the weight of the robot, respectively. With the robot approximately being 10 lbf, this equates to 30 lbf and 5 lbf for the vertical force and the horizontal force, respectively [5]. Using these forces and assuming the lengths of the rod and tube to be 12 inches long, the moment was found for an 8 spoke design. Then, Equation A11, Equation A12, and Equation A13 were used in conjunction with the geometry of the rimless wheel (Figure A14) to find the bending, axial, and shear stresses, respectively. The direction of the print also plays a factor in the strength of the design because it weakens the design by a large factor. Lacking reputable scientific resources for analysis of weaknesses introduced to FDM 3D parts through printing direction, the team looked into a material with similar weaknesses along the grain: wood. Researching into the loss of strength of wood because of the grains, it is seen that the grains weaken the wood's strength by a factor of 20 to 30 [16]. This was done for both the in phase configuration and the out of phase configuration. These values are shown in Table A7 and Table A8 for the rod and Table A9 and Table A10 for the tube for the in phase and out of phase configurations, respectively [5].

These calculations show that the shear stress is the main factor in that leads to failure for the tube and the bending stress is the main factor for the rod. Therefore, these should be used as the basis for the factor of safety. The radii of the rod and tube were changed until a safety factor of

about 2 was achieved (Table A11). The safety factors were calculated using the Modified Goodman Criteria shown in Equation A15 and shown in Table A11. The stress amplitude and the midrange stress are both half of the bending stress because the stress goes from 0 to the calculated bending stress. The Endurance strength of the material was calculated using Equation A14. Table A11 also shows the fatigue cycles each part will be able to sustain. These were calculated using Equation A16.

The design needs certain requirements in the amount of torque and power needed to start or continue movement. Based on some simple calculations of the minimum amount of torque needed to start the design, the minimum torque needed to start the design with 8 spokes is about 45 in-lb (Figure A14). After that starting torque, the robot would continually need less power to continue motion due to the forward momentum that it gains from motion. Based on the data from Table A4, the amount of torque needed to continue at the specified speed is around 5-6 in-lb. The minimum speed the motor must output is 90 RPM under the load of the robot's weight. This rotational speed corresponds to 4 MPH which is the minimum speed that the robot must accomplish based on the specification set by our sponsor/mentor. Using these values, a proper motor and batteries were chosen such that enough power is obtained.

As a result of these calculations, the Roadrunner Robot has achieved expected performance with respect to the failure prevention of the design, the deflection of the spring, and the amount of power that would be required to propel itself. The final design has been shown through testing to meet the design specifications declared at the beginning of the Roadrunner Project. The design was made to be open to modification for further research on legged locomotion in robotics in the Robotics and Motion Laboratory at UTSA.

8. Fabrication

To facilitate ease of modification and variability in the final design, over half of the robot is 3D printed using ABS plastic. For the driving components requiring more strength, the team relied

on the UTSA machine shop to cut the required steel and aluminum pieces. Both the 3D printing personnel and machinists completed all required work in a timely manner and free of charge.

8.1. 3-D Printing

3-D printing was chosen as the main mode of fabrication because of its cheap additive manufacturing cost, short lead time for rapid prototyping, and its use of lightweight plastic. The team chose to use ABS plastic material in combination with the *Stratasys Dimension 1200es* 3-D printer provided by Dr. Hung-da Wan and the Flexible Manufacturing and Lean Systems Laboratory at the University of Texas at San Antonio because of its printing resolution, and unlike other 3-D printers located at the school the printer makes solid infill parts rather than honeycomb structure, which aids in mechanical loading. Dr. Hung-da Wan has also offered printing free of charge, reducing the material cost of the project [17].

The beginning of fabrication of the robot started with determining the printing direction of each part to be printed. With the *Stratasys Dimension 1200es* printer, 3-D printed objects have a grain direction because the printer extrudes one layer at a time with each layer adhered to the next. The joints between layers are susceptible to delamination and can become weak points if the layering direction of the object is not chosen deliberately to minimize the chance of delamination. Because the robot will endure mechanical loading, grain direction and thickness of parts were considered when designing. The case, case lid, and motor mount were determined to take the least amount of load making grain directions of the parts insignificant compared to thickness. Thickness of each part were adjusted to withstand its respective load, while the grain directions were chosen to reduce the chance of delamination. The rod and tubes' printing direction was chosen to be collinear with the length of parts as they will endure dynamic load from the motion of the robot, in addition to the weight of the robot. By arranging the grain direction to be collinear with the length of the rod and tube, possible delamination from forces introduced by impact collisions will be reduced.

Preliminary testing of the printer accuracy was conducted to determine a fitment for the spoke assembly that allows the rod to slide freely inside of the tube while minimizing clearance. The first preliminary testing of the rod and tube fit was designed to have a loose running fit (H11/c11) with a basic hole size of 0.5” based on ANSI standards using the Basic Hole System resulting in a clearance of 0.013”; the rod failed to fit inside the tube due to the printer resolution. A second test for the rod and tube was conducted using the printer’s layer thickness of 0.1” as a basis for finding the desired clearance size. A single rod with a diameter of 0.5” and 5 tubes of increasing inner diameter in intervals of 0.01” starting at 0.5” were printed. The rod failed to fit into 0.50”, and the 0.51” tube had an interference fitment. The rod was able to fit into the 0.52” tube akin to a transition fit however, for the spoke assembly a clearance fit was needed. Because of this, the team chose the 0.53” test tube as the 0.03” clearance satisfied the requirements of running freely inside of the tube and have the minimal clearance the printer is capable of. From this, the final design of the rod was designed with a diameter of 0.64” and the tube inner diameter of 0.67” to contain the 0.03” clearance between the rod and tube in the spoke assembly. In the rimless wheel sub assembly, hub pegs that connect to the tubes of the spokes have a diameter of 0.65” to have a 0.02” clearance between peg and tube, for a compromise between clearance and interference fit.

The first hub design was made to be a circular body with pegs extending radially attach to the spokes. The end of the spoke attaching to the pegs were designed to match the circular body of the hub. After examining the first prototype of the spoke assembly, imperfections in the printer’s ability to print out small curved edges, it was decided that the hub be redesigned into a octagonal body and the end of the spoke be redesigned flat to match the octagonal body as well as avoid the issue of the printer’s inability to make small curved edges.

Bearings were press fitted into the sides of the case to dissociate the axle’s rotational motion from the case. The design of the bearing holes require the bearings stay rigid and not move relative to the case while also be easily removable to be replaced. A testing fixture (Figure A20) with 6 hole sizes of increasing hole diameter in intervals of 0.005” with a basic size of 7/16” (0.4375”) was printed to evaluate the bearing hole size. The bearing was fitted into each

hole, leading the team to choose 0.4425” diameter hole as it stayed rigid in the test block and was easily removable.

8.2. Machining

Due to the extensive use of 3D printing for the individual parts of the Roadrunner Robot, only 4 unique parts needed custom machining. To facilitate the machining, the team worked closely with Paul Krueger and David Kuenstler in the machine shop at the University of Texas at San Antonio. The first and highest priority parts to be machined were the axle and the flange so the team could complete a rolling assembly and begin passive rimless wheel testing by the beginning of March. Then, after the team received the motor, both the pinion gear and the spur gear were machined to be compatible with the motor and axle components.

For the machining of the axle (DWG NO. B-B-AX210), a plain steel round rod with a length of 36” and a diameter of .25” was provided to the machinist. The rod was first cut to length and then drilled thru and threaded for #4-40 bolts. The team also provided Paul Krueger with 6061-T6 Aluminum disc stock with a diameter of 3” to be used for the machining of the two flanges (DWG NO. M-AL-FL01). The stock was first turned down to the exact diameter and width and then placed in the CNC machine to have the intricate curves and holes machined precisely.

8.3. Ordered Parts

Aside from the 3D printed and machined parts, the team was able to order the majority of the parts and use them “off the shelf” for the final assembly. For the rimless wheel, the only parts that required ordering include the rubber boot for the end of the tube (SKU: 762 099), the springs (Part No. 9657K254) and the #4-40 screws with washers and a nylon lock nuts. For the connection of the rimless wheel to the body of the robot, it was necessary to order the larger #6-32 bolts with matching washers and nuts and the needle roller bearings (Part No. SCE45). In addition the aluminum stock for the flange and steel stock for the axle were ordered and machined to the specified dimensions. Two of the ordered parts that required machining were the pinion gear (Part No. A 6A 6-10DF03104) and the spur gear (Part No. A 6Z61-20DF02508). Originally, the team’s plan was to use the pinion gear off the shelf with a bore size of .125”, but

due to receiving the wrong size shaft for the motor (5mm instead of the supplier claimed .125”), a new pinion gear was ordered and the bore was then matched to the metric 5mm diameter of the motor shaft. For the spur gear, the team chose to have the screw threaded thru the entire length of the hub for added strength. Because the spur gear hub already had a set screw hole, Paul maintained the same hole size but drilled it thru. The axle set screw going thru the diameter of the spur gear hub provided the added strength the team was seeking for the rotating assembly. To transfer the rotation of the drive gear to the spur gear, a timing belt was ordered (Part No. A 6R 6-1320250).

The body of the robot contained the majority of the ordered parts. These included the Tekin brushless motor (Part No. TT2369), which receives its power from two 11.1 volt, lithium polymer batteries. All of the ordered parts received by the team arrived on time and without error with the exception of the misrepresented motor shaft size.

8.4. Assembly

As the design of the Roadrunner Robot developed, the team made the future ease of assembly, repair and maintenance for the Robotics and Motions Laboratory personnel a high priority. The robot uses modular subassemblies to minimize the amount of assembly and disassembly required for replacing or removing parts.

8.4.1. Rimless Wheels

The methods to assemble the rimless wheels depends on whether the user wants to run the robot in-phase, anti-phase, or variable-phase. The beginning instructions for the assembly are the same for each scenario. To assemble the spoke, slide the SPRING onto the end of the ROD with the slot. Next, prepare a #4 - 40 BOLT by first sliding a #4 screw size WASHER onto the bolt, then slide the BUSHING onto the BOLT. Use the wide end of the TUBE to compress the SPRING until the hole on the TUBE matches with the slot. Continue by pushing the BOLT through the hole and slot to lock the ROD and TUBE together with the sliding bolt in slot mechanism. Next, secure the #4 - 40 BOLT with another WASHER and a #4 -40 NUT and attach the RUBBER LEG TIP onto the rod. Repeat the above steps for each of the 16 spokes. To attach the spoke to the hub, attach the TUBE end of the SPOKE to one of the pegs which extend from the HUB &

align the holes. Next, secure the SPOKE to the HUB with two #4 - 40 size WASHERS, a BOLT, a BUSHING and a NUT. Repeat steps 1-3 for each of the eight pegs to assemble a LEG and repeat all of the previous steps to assemble the second LEG (Figure 5).

For the various phases of the spokes, there are slightly different assembly instructions. If the user seeks to create an in-phase arrangement, begin by aligning the HUB with the FLANGE such that the holes on the FLANGE align with the holes on the HUB. Next, secure 4 holes of the HUB to the FLANGE with #6 - 32 BOLTS, WASHERS, and NUTS. Repeat above steps for the 2nd LEG making sure to use the same holes used on the first LEG (either both legs secured at point C or both secured at point D). If the user seeks to create an anti-phase arrangement, align the HUB with the FLANGE such that the holes on the FLANGE align with the holes on the HUB. Continue by securing 4 holes of the HUB to the FLANGE with #6 - 32 Bolts, WASHERS, and NUTS. Repeat the above steps for the second LEG using the holes on the HUB to align the LEG so that it is opposite the first LEG (one leg at point C and the other at point D). Finally, if the user seeks to create a variable phase arrangement, Align all 4 holes of LEG to the slots on the FLANGE until the phase angle between legs that is desired is achieved. Secure all 4 holes of the LEG to the FLANGE with #6 - 32 Bolt, WASHERS, and NUTS. Construct the second leg as normal, using the circular holes on the FLANGE (Figure 6).

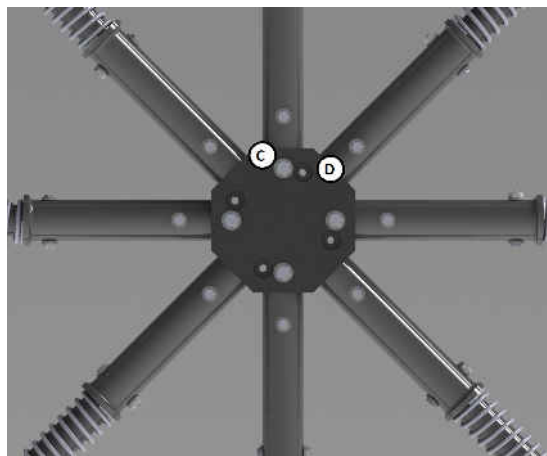


Figure 6: Phase Arrangement



Figure 5: Spoke Assembly

8.4.2.Body

The body of the Roadrunner Robot consist of two major components, the microcontroller assembly and the motor with mounting hardware. For the microcontroller assembly, place the ZIGBEE MODULE on the ZIGBEE SHIELD by connecting the pins of the chip to the female sockets of the shield at the location on the shield with the ZIGBEE SHIELD chip outline. Next, mount the shield on the ARDUINO MEGA 2560, making sure that the 6 ICSP pins are aligned with the shield's female mates correctly, and that the shield's side pins align with the female mates on the Arduino. To complete the motor assembly, Slide MOTOR shaft through the large central hole on the MOTOR PLATE with the wire terminals of the MOTOR pointed away from the MOTOR PLATE. Continue by aligning the holes of the MOTOR PLATE and the MOTOR and secure the MOTOR to MOTOR PLATE with the 3mm SCREWS provided by the MOTOR manufacturer. Finally, slide the PINION GEAR halfway onto the MOTOR shaft and secure the PINION GEAR onto the motor shaft with the SETSCREW (Figure A17).

8.4.3.Robot Assembly

To complete the final assembly of the Roadrunner Robot, some final assembly steps are required. Begin by pressing the BEARINGS into the BEARING HOUSINGS on the sides of the case until the bearings seat flush with the edge of the case. Next, slide the AXLE through one side of the case and slide the SPUR GEAR with the set screw hole facing the right side of the case. Continue by sliding the TIMING BELT onto the AXLE and securing the SPUR GEAR onto the AXLE with the #6 - 32 BOLTS, NUTS, and WASHERS, such that the TIMING BELT lays

against the SPUR GEAR. Next, slide the AXLE through the other side of the case and slide the FLANGES with LEGS ATTACHED onto either end of the AXLE until the AXLE comes into contact with the HUB. Continue by aligning the hole on each end of the AXLE with the hole on each FLANGE and secure with #4 - 40 BOLT, WASHERS and NUT. Also, align the PINION GEAR on the MOTOR with the SPUR GEAR and secure the Pinion gear onto the motor shaft with the SETSCREW. Next, place the TIMING BELT onto the SPUR GEAR and PINION GEAR and align the holes on the



bottom of the MOTOR PLATE to the slots on the MOTOR MOUNT inside of the case. Pull the MOTOR PLATE along the slot until the TIMING BELT is tightened, then loosely secure the MOTOR PLATE with #6 - 32 BOLTS, NUTS, and WASHERS. Seven 2" x 1" strips of VELCRO must be cut and before separating the loop and hook sides. Place two strips of VELCRO hooks in a line on the back wall of the battery holder located at the bottom of the case and place two VELCRO loops on the thin side of the first LiPo BATTERY to match the VELCRO hooks on the back wall of the case. The battery must be set in the case such that the battery connectors come out the left side. Continue by placing two strips of VELCRO hooks in a line on the bottom of the case next to the first battery installed and placing two VELCRO loops on the bottom of the second LiPo BATTERY to match the VELCRO hooks on the bottom of case. Also, place the second LiPo BATTERY on the VELCRO loops so that the battery connectors come out the same side as the first battery and center two VELCRO hooks on top of the battery shelf. On top of the battery shelf, place a VELCRO loop on the center bottom of the ESC and place the ESC on the left side. Place a VELCRO loop to match the VELCRO hook on

the top of the battery shelf and place the 9V battery case an inch to the right of the ESC and center one VELCRO hook on the right wall of the case 2" above the top of the battery shelf. Finally, place a VELCRO loop on the back of the ARDUINO MEGA to match the VELCRO hook on the right wall and mount the ARDUINO MEGA to the right wall such that the USB port faces towards the sky. To complete the assembly, place the CASE LID onto the CASE and align the holes. Use a #4-40 SCREW, WASHERS on either side of the hole, and a NUT to secure the lid on the case at each of the four holes (Figure 7).

9. Testing

Following the fabrication of the Roadrunner Robot, testing was conducted to verify that the parts and assemblies met the design specifications, and that the robot was able to meet the minimum performance requirements (Figure 8).

Requirements		Tolerance as Stated in Drawing Package	Max Height 2 ft.	Max Width 1.5 ft.	Less than 15 lbs	Battery Powered	Utilizes Springs	Motor Driven	Rimless Wheel Design	Reduce Energy Lost to Hard Collisions	Velocity Exceeding 4MPH	Remote Controlled From Atleast 50 ft.	Dynamically Stable
		Tests											
Specifications	Measure	✓	✓	✓									
	Scale				✓								
	Visual					✓	✓	✓	✓				
Functional Requirements	Passive Energy Balance									✓			
	Driving					✓	✓	✓	✓		✓	✓	✓

Figure 8: Traceability Matrix

9.1. Satisfying (functional) specifications

9.1.1. Remote Control

Specification: The radio frequency remote control will transmit motor commands to the microcontroller to control the motor speed. The remote control must have a minimum operational range of 50 feet.

Verification Method: The operational range of the remote control is tested by issuing commands from the controller and verifying that the robot is outputting those commands. The test is conducted with minimal obstructions (walls) between the operator and the robot.

Results: The testing was concluded when the robot reached 150 feet (300% of minimum requirement) and still received commands.

9.1.2. Speed

Specification: The robot must achieve a linear velocity of at least 4 miles per hour.

Verification Method: The average velocity of the robot is taken by running the robot at steady state while measuring the linear distance covered and the time elapsed. The average velocity is the ratio of linear distance with time elapsed. Several trials are conducted to ensure that reliable data is produced.

Results: The robot was found to have a maximum recorded velocity of 5.84 miles per hour at 20% of maximum power (Figure).

9.2. Satisfying physical requirements

9.2.1. Dimensions

Specification: The dimensions of the machined and printed parts must be verified using a Vernier caliper or scale. The dimensions of the assembly (diameter and width) should be recorded only after the entire assembly is completed. If the part dimensions have been verified and proper assembly instructions are followed, the robot will have a maximum diameter of 2 feet and maximum width of 1.5 feet.

Verification Method: The parts are measured using a Vernier caliper or a scale, depending on the size and resolution required.

Results: The parts and assembly were found to be within allowable tolerances (Table A16 & Figure A11).

9.2.2. Weight

Specification: The weight of the robot must not exceed 15 lbs, including all electrical components.

Verification Method: The assembly is weighed using a weighing scale to verify that the robot's weight is under the specified value.

Results: The robot weighs approximately 8 lbs (53.3% of maximum weight).

9.3. Validation of Results

To validate that the collected data is accurate, the measurement tools will be inspected and calibrated if necessary before each test. For tests with multiple data points, the measurement tool should not be calibrated between trials. In the event that a tool is found to be miscalibrated

between trials, the test operator will evaluate the magnitude of the miscalibration and determine if a fresh test is required.

10. Project Management

10.1. Personnel

This project has many demanding requirements in fields that Mechanical Engineering majors do not experience in depth. These fields include the research, design and operation of electrical components and the coding associated with controlling those electrical components. Additionally, aspects of mechatronics and robotics including motor design decisions, implementing robust control systems, and assembly of the robot are required. Since the team lacks members experienced in robotics and dealing with electronic components, this project presents many possible challenges to the team for the design and fabrication of the robot. To help the team overcome these challenges, Dr. Pranav Bhounsule has agreed to mentor and sponsor the team. In addition to his extensive experience in developing and testing walking robots, Dr. Pranav is providing the team with access to the Robotics and Motion Laboratory at UTSA.

Scott Miller is the CAD Specialist and has skills in SolidWorks, technical writing and coding. Rico Jovanni Ulep is the team leader and has skills in leading the team, MATLAB, SolidWorks, and analysis. Ezra Ameperosa is the design specialist and carries the most experience in coding. In addition, he has skills in formatting, and critical thinking. Kyle Seay deals with fabrication and has skills in assembly and troubleshooting.

10.2. Overall Schedule

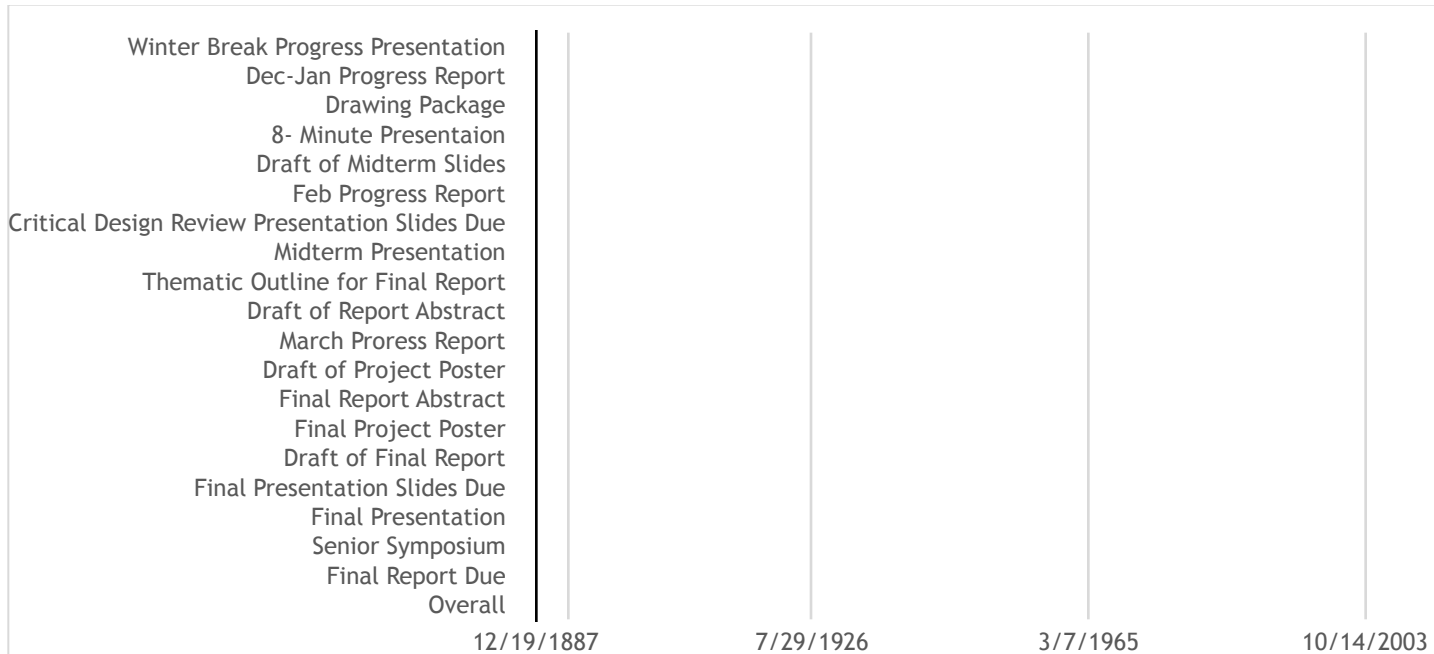


Figure 9: Senior Design 2 Schedule

Figure 9 shows that all tasks have been completed. Overall, the entire project was completed on schedule.

10.3. Personnel Assignments

In addition to the significant efforts expended by the team in researching and designing throughout the first semester of Senior Design, each member has a list of individual responsibilities to ensure timely completion of the project. Scott is responsible for preparing all SolidWorks models of parts and assemblies of the robot. He has worked in tandem with Ezra in coding the remote controller. Scott also proves to be a great boon in writing and editing major deliverables. Rico ensures everyone in the group stays on task and provides leadership by making decisions and solving problems. In addition, he is responsible for the analysis that has been done to make sure that the robot functions as expected. He also works with Scott to draft all engineering drawings. Ezra's responsible for most of the coding of the remote control and the radio frequency transmission between it and the robot. In addition, he was responsible for calculating cost and finding parts for the final design of the robot. Ezra is also skilled in formatting the major deliverable keeping them neat. Kyle worked closely with the machine shop

ensuring that all machined parts were easily manufactured. Kyle also worked in the assembly of the robot troubleshooting any problems that arose.

10.4. Financial Performance

At the end of Senior Design, the project was under budget. Since the project was completed and tested by the deadline that was established at the beginning of the semester, the project is fully on schedule. The project has wound up under budget because of the overestimated amount of hours that needed to be put in at the beginning of the semester. Figure 10 shows the project costs and budget based on fully loaded industry rates. Table 1 shows the cost analysis for the project. The project's CPI, SPI, and CSI are 1.15, 1.00, and 1.15, respectively. It also shows the BCWS, ACWP, and BCWP. These further prove that the project was completed under budget and on schedule.

10.4.1. Overall Planned Cost vs. Time compared to Actual Cost vs. Time

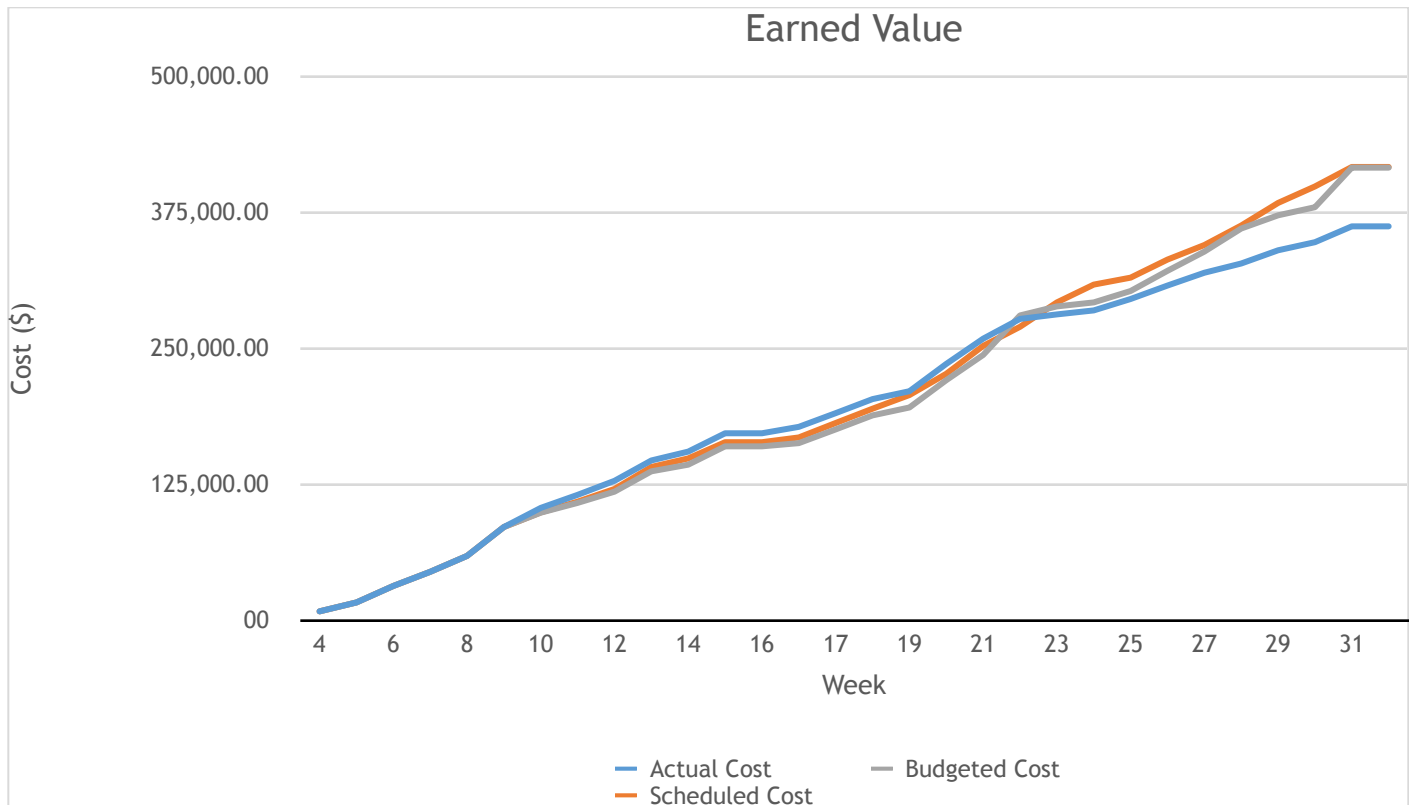


Figure 10: Earned Value Chart (Based on Fully Loaded Industry Rates)

Table 1: Cost Analysis

CPI	1.15
SPI	1.00
CSI	1.15
BCWS	416788.75
ACWP	362167.45
BCWP	416150.84

11. Conclusions

Force Over Area Engineering has successfully developed Roadrunner, the rimless wheel robot. The robot uses 3D printing for most of its parts and is designed to be modular and versatile to allow a greater spectrum of data to be collected. The prototype robot passed several tests to verify that the prototype met the robot's design requirements. The Roadrunner Robot will be used for research focusing on legged locomotion and rimless wheel technology in the Robotics and Motions Laboratory at UTSA. The data collected from this research will bolster the academic community's limited understanding of rimless wheel technology and may have application in terrestrial and extraterrestrial scouting of rough terrains.

12. Future Work

The testing that the Roadrunner has conquered so far was limited to the scope of validating the prototype. Future testing will take advantage of the versatility of the design to compare the energy efficiency of different spoke configurations, springs, terrains, and velocities. The Roadrunner prototype robot will be attending the international 2015 Dynamic Walking conference at Ohio State University in July, where it will show off and socialize with other robots.

13. References

- [1] "Percentage Change." *Percentage Change*. Math Is Fun, n.d. Web. 24 Nov. 2014. <<http://www.mathsisfun.com/numbers/percentage-change.html>>.
- [2] Coleman, Michael Jon. A Stability Study of a Three-Dimensional Passive -Dynamic Model of Human Gait. Diss. Cornell U, 1998. N.p.: n.p., n.d. Print.
- [3] Ruina, Andy, John Bertram, and Manoj Srinivasan. "A Collisional Model of the Energetic Cost of Support Work Qualitatively Explains Leg Sequencing in Walking and Galloping, Pseudo-elastic Leg Behavior in Running and the Walk-to-run Transition." Science Direct. *Journal of Theoretical Biology*, 14 June 2005. Web. <http%3A%2F%2Fac.els-cdn.com%2FS0022519305001591%2F1-s2.0-S0022519305001591-main.pdf%3F_tid%3D651870e2-73a3-11e4-88ac-00000aacb35e%26acdna%3D1416810814_d53acbf96c94b39779eafc10bac54c03>.
- [4] Nagurka, M., and S. Huang. "A Mass-Spring-Damper Model of a Bouncing Ball." A Mass-Spring-Damper Model of a Bouncing Ball (n.d.): n. pag. Web. <http://www.eng.mu.edu/nagurka/NagurkaHuang_MassSpringDamperModelBouncingBall_ACC04.pdf>.
- [5] Cavanagh, Peter R., and Mario A. Lafortune. "Ground Reaction Forces in Distance Running." *Biomechanics* 13 (1980): 397-406. Pergamon Press Ltd. Web. 24 Nov. 2014. <[http://www.uta.edu/faculty/ricard/Classes/KINE-5350/Cavanagh%20\(1980\)%20Ground%20reaction%20forces%20in%20distance%20running%20.pdf](http://www.uta.edu/faculty/ricard/Classes/KINE-5350/Cavanagh%20(1980)%20Ground%20reaction%20forces%20in%20distance%20running%20.pdf)>.
- [6] CNN Library. "Oscar Pistorius Fast Facts." CNN. Cable News Network, 07 Nov. 2014. Web. 26 Nov. 2014. <<http://www.cnn.com/2013/03/06/world/africa/oscar-pistorius-fast-facts/>>.
- [7] "Inside Asimo." Inside ASIMO Robotics by Honda. N.p., n.d. Web. 26 Nov. 2014. <<http://asimo.honda.com/Inside-ASIMO/>>.
- [8] "Moment of Inertia: Cylinder." *Hyper Physics*. N.p., n.d. Web. <<http://hyperphysics.phy-astr.gsu.edu/hbase/icyl.html#icyl>>.
- [9] "Rotational Energy." *Wikipedia*. Wikimedia Foundation, 30 Nov. 2014. Web. 07 Dec. 2014. <http://en.wikipedia.org/wiki/Rotational_energy>.

- [10] "Ahmed Mogahed." *Mass Spring Damper System*. N.p., n.d. Web. 07 Dec. 2014. <<http://www.ahmedmogahed.me/tutorials/mass-spring-damper/>>.
- [11] "Coulomb Damping." Rose-Hulman Institute of Technology, n.d. Web. 7 Dec. 2014. <https://www.rose-hulman.edu/~cornwell/courses/em406/em406_lectures/lecture%205%20-%20coulomb%20damping.pdf>.
- [12] Budynas, Richard G., and J. Keith Nisbett. *Shigley's Mechanical Engineering Design Connect Access Card to Accompany Mechanical Engineering Design*. 9th ed. New York: McGraw-Hill Science Engineering, 2010. Print.
- [13] "Acrylonitrile Butadiene Styrene (ABS) Typical Properties Generic ABS." *Plastics*. N.p., n.d. Web. 07 Dec. 2014. <<http://plastics.ulprospector.com/generics/1/c/t/acrylonitrile-butadiene-styrene-abs-properties-processing>>.
- [14] Orban, F. "Damping of Materials and Members in Structures." *IOP Science*. N.p., n.d. Web. 7 Dec. 2014. <http://iopscience.iop.org/1742-6596/268/1/012022/pdf/1742-6596_268_1_012022.pdf>.
- [15] Arslan, Omur. "Spring Loaded Inverted Pendulum (SLIP) Approximate Stance Map for Nonsymmetric Motions and Variable Stiffness." Diss. Bilkent U, 2008. Spring Loaded Inverted Pendulum (SLIP) Approximate Stance Map for Nonsymmetric Motions and Variable Stiffness. 07 July 2008. Web. 29 Apr. 2015. <http://bdrl.ceng.metu.edu.tr/_media/publications/bu-tr-00001.pdf?id=publications%3Aintro&cache=cache>.
- [16] Green, David W., Jerrold E. Winandy, and David E. Kretschmann. "Mechanical Properties of Wood." *Wood Handbook--Chapter 4--Mechanical Properties of Wood* (n.d.): n. pag. Web. 29 Apr. 2015. <<http://www.conradfp.com/pdf/ch4-Mechanical-Properties-of-Wood.pdf>>.
- [17] "Dimension 1200es." 3D Modeling Printers| Stratasys. N.p., n.d. Web. 29 Apr. 2015. <<http://www.stratasys.com/3d-printers/design-series/dimension-1200es>>.

14. Appendix A

Equation A1: Mass Moment of Inertia of a Rod about the Central Axis (reference [8])

$$I = \frac{1}{2}MR^2$$

M = Mass

R = Radius of Cylinder

Equation A2: Mass Moment of Inertia of a Rod about the End of the Rod (reference [8])

$$I = \frac{1}{4}MR^2 + \frac{1}{3}ML^2$$

M = Mass

R = Radius of Cylinder

L = Length of Cylinder

Equation A3: Percent Change (reference [1])

$$\frac{\text{New Value} - \text{Old Value}}{|\text{Old Value}|} \times 100\%$$

Equation A4: Passive Rimless Wheel Energy Loss after One step (reference [2])

= Angular velocity after the collision/step

= Angular velocity before the collision/step

I_c = Mass moment of inertia about the center of the rimless wheel

m = Mass

= Radius of the rimless wheel

n = Number of Spokes

Equation A5: Rotational Energy (reference [9])

$$E_{\text{rotational}} = \frac{1}{2}I\omega^2$$

I = Mass moment of inertia

= Angular speed

Equation A6: Equation of Motion of Collision (references [10] & [11] & [4])

$$m\ddot{x} = -kx - F_d \operatorname{sgn}(\dot{x}) - c\dot{x} - mg$$

x = Position from equilibrium
= Velocity
= Acceleration
m = Mass of leg
k = Spring rate
c = Damping coefficient
= Friction force
sgn() = Sign or signum function
F(t) = Forcing function
g = Gravity

Equation A7: Coefficient of Generation [3]

$$e_g = \frac{e_r - 1}{e_r + 1}$$

eg = Coefficient of generation
er = Coefficient of restitution

Equation A8: Energy cost based on Coefficient of Generation [3]

$$= \frac{\phi^2 v^2 m}{8} (1 - r)(1 - e_g)^2.$$

E = Energy cost
= Contact angle
V = Velocity
m = Mass
r = Elastic recovery
eg = Coefficient of generation

Equation A9: Energy Ratio of Passive and Springed Rimless Wheel [3]

$$\frac{E_{Spring}}{E_{Passive}} = \frac{(1 - e_{gOfSpring})^2}{(1 - e_{gOfPassive})^2}$$

E = Energy cost
eg = Coefficient of generation

Equation A10: Coefficient of restitution of a spring damper system during collision [4]

$$e = \left| \frac{\dot{x}(\Delta T)}{\dot{x}(0)} \right| .$$

e = Coefficient of restitution
= Velocity
t = Time

Equation A11: Bending Stress (reference [12])

s = Stress
M = Moment
y = Distance from the neutral axis
I = Second moment of area

Equation A12: Axial Stress (reference [12])

s = Stress
F = Axial force
A = Cross sectional area

Equation A13: Shear Stress (reference [12])

s = Stress
V = Shear force
A = Cross sectional Area

Equation A14: Endurance Strength (reference [12])

S_e = Endurance limit at the critical location of a machine part in the geometry and condition of use

k_a = Surface condition modification factor

k_b = Size modification factor

k_c = Load modification factor

S_e' = Rotary-beam test specimen endurance limit

Equation A15: Modified Goodman Fatigue (reference [12])

Mod. Goodman Fatigue Factor of safety

$$n_f = \frac{1}{\frac{\sigma_a}{S_e} + \frac{\sigma_m}{S_{ut}}}$$

n_f = Fatigue Factor of Safety

σ_a = Stress Amplitude

σ_m = Midrange Stress

S_e = Endurance Strength

S_{ut} = Tensile Strength

Equation A16: Cycles to failure (reference [12])

$$S_f = a * N^b$$
$$a = \frac{(f * S_{ut})^2}{S_e}$$
$$b = -\frac{1}{3} * \log\left(\frac{f * S_{ut}}{S_e}\right)$$

S_f = Fatigue Strength

N = Number of cycles

S_{ut} = Ultimate tensile strength

S_e = Endurance strength

Equation A17: SLIP System Equation of Motion

$$\mathbf{q} = \begin{bmatrix} q_\theta \\ q_\phi \\ q_r \\ q_{\dot{r}} \end{bmatrix}$$

$$\dot{\mathbf{q}} = \begin{bmatrix} \dot{q}_\theta \\ \dot{q}_\phi \\ \dot{q}_r \\ \dot{q}_{\dot{r}} \end{bmatrix} = \begin{bmatrix} q_\phi \\ -\frac{g_s \sin(q_\theta)}{q_r} - \frac{2q_r q_\phi}{q_r} \\ q_{\dot{r}} \\ \frac{F_s(q_r, q_{\dot{r}})}{m} + q_r q_\phi^2 - g_s \cos(q_\theta) \end{bmatrix}$$

$$F_s(q_r, q_{\dot{r}}) = \begin{cases} k_c(l_0 - q_r) & , \text{ if } q_{\dot{r}} \leq 0; \\ k_d(l_0 - q_r) & , \text{ if } q_{\dot{r}} > 0. \end{cases}$$

Leg & Body Coordinates	
q_r	Leg Length
q_θ	Leg angle from Vertical (counterclockwise convention)
q_ϕ	Leg Compression rate
q_ψ	Leg Swing rate
p_r	Radial Momentum
p_θ	Angular Momentum
b_x	Horizontal Position of Body
b_y	Vertical Position of Body
$b_{\dot{x}}$	Horizontal Velocity of Body
$b_{\dot{y}}$	Vertical Velocity of Body
p_x	Horizontal Momentum
p_y	Vertical Momentum
b_{t_0}	Horizontal Position of Toe
SLIP Parameters	
m	Body Mass
l_0	Rest Length of Springy Leg
k	Spring Constant used for general formulation
k_c	Compression Phase Spring Constant
k_d	Decompression Phase Spring Constant
g_s	Gravitational Acceleration during stance phase(positive)
g_f	Gravitational Acceleration during flight phase(positive)
$F_g(x)$	Ground function. For a given position x, it returns the ground height.
$F_s(r, \dot{r})$	Spring force function. For a given leg length it returns spring force based on the stance phase of SLIP.
$U_s(r, \dot{r})$	Spring potential energy function. For a given leg length it returns stored energy on compliant leg based on the stance phase of SLIP.
E	Total Mechanical Energy
Touchdown Parameters	
$q_{\theta t}$	Leg Angle at Touchdown
$q_{r t}$	Leg Length at Touchdown
Liftoff Parameters	
$q_{\theta o}$	Leg Angle at Liftoff
$q_{r o}$	Leg Length at Liftoff
Apex Parameters	
b_{i_a}	Apex Velocity
b_{h_a}	Apex Height

Table A2: Mass Moment of Inertia Approximations

Mass Moments Of Inertia Approximations	
	I (lbm*in ²)
Rod about Central Axis	0.0443
Rod about its End	17.032
4 Spokes per Side	68.1723
5 Spokes per Side	85.2043
6 Spokes per Side	102.2363
7 Spokes per Side	119.2683
8 Spokes per Side	136.3003
9 Spokes per Side	153.3323
10 Spokes per Side	170.3643
11 Spokes per Side	187.3963
12 Spokes per Side	204.4283
13 Spokes per Side	221.4603
14 Spokes per Side	238.4923
15 Spokes per Side	255.5243
16 Spokes per Side	272.5563
17 Spokes per Side	289.5883
18 Spokes per Side	306.6203
19 Spokes per Side	323.6523
20 Spokes per Side	340.6843

Table A3: Mass Approximations

Mass Approximations	
	M (lbm)
Spoke	0.3544
Shaft	0.3544
4 Spokes per Side	1.772
5 Spokes per Side	2.1264
6 Spokes per Side	2.4808
7 Spokes per Side	2.8352
8 Spokes per Side	3.1896
9 Spokes per Side	3.544
10 Spokes per Side	3.8984
11 Spokes per Side	4.2528
12 Spokes per Side	4.6072
13 Spokes per Side	4.9616
14 Spokes per Side	5.316
15 Spokes per Side	5.6704
16 Spokes per Side	6.0248
17 Spokes per Side	6.3792
18 Spokes per Side	6.7336
19 Spokes per Side	7.088
20 Spokes per Side	7.4424

Table A4 Energy Loss

mu	Spokes per Side	Initial Angular Vel (rad/s)	Final Angular Vel (rad/s)	Initial Energy (in-lb)	Final Energy (in-lb)	Energy lost (in-lb)
0.229	4	7.333333333	1.68	4.74	0.25	4.50
0.47	5	7.333333333	3.45	5.93	1.31	4.62
0.618	6	7.333333333	4.53	7.11	2.72	4.40
0.713	7	7.333333333	5.23	8.30	4.22	4.08
0.777	8	7.333333333	5.70	9.48	5.73	3.76
0.822	9	7.333333333	6.03	10.67	7.21	3.46
0.855	10	7.333333333	6.27	11.86	8.67	3.19
0.88	11	7.333333333	6.45	13.04	10.09	2.95
0.899	12	7.333333333	6.59	14.23	11.48	2.74
0.913	13	7.333333333	6.70	15.41	12.85	2.56
0.925	14	7.333333333	6.78	16.60	14.20	2.39
0.935	15	7.333333333	6.85	17.78	15.54	2.25
0.943	16	7.333333333	6.91	18.97	16.85	2.12
0.949	17	7.333333333	6.96	20.15	18.15	2.00
0.955	18	7.333333333	7.00	21.34	19.44	1.90
0.959	19	7.333333333	7.03	22.52	20.72	1.80
0.963	20	7.333333333	7.06	23.71	21.99	1.72

Table A5: Remaining Energy per Mass

Spokes per Side	Percent of Energy Remaning	(Percent Energy Remaining) / (Mass) (1/lbm)
4	5.24%	0.03
5	22.08%	0.10
6	38.17%	0.15
7	50.82%	0.18
8	60.39%	0.19
9	67.62%	0.19
10	73.12%	0.19

11	77.39%	0.18
12	80.73%	0.18
13	83.41%	0.17
14	85.58%	0.16
15	87.37%	0.15
16	88.83%	0.15
17	90.06%	0.14
18	91.11%	0.14
19	91.99%	0.13
20	92.76%	0.12

Table A6: Energy Cost Comparison between Springed and Passive Rimless Wheel

Mass (lbm)	Spring Stiffness (lbf/in)	Damping Coefficient (lbf*s/in)	Initial Velocity (fps)	Final Velocity (fps)	er	eg	Percent energy increase from plastic collisions
10	10	5.60	22	12.072	0.549	-0.2914	41.69%
10	20	6.01	22	13.970	0.635	-0.2232	37.41%
10	30	6.33	22	14.818	0.674	-0.1951	35.70%
10	40	6.60	22	15.341	0.697	-0.1783	34.71%
10	10	5.60	15	7.904	0.527	-0.3098	42.89%
10	20	6.01	15	9.350	0.623	-0.2320	37.95%
10	30	6.33	15	9.990	0.666	-0.2005	36.03%
10	40	6.60	15	10.376	0.692	-0.1822	34.94%
10	10	5.60	9	4.255	0.473	-0.3580	46.10%
10	20	6.01	9	5.354	0.595	-0.2540	39.31%
10	30	6.33	9	5.814	0.646	-0.2151	36.91%

10	40	6.60	9	6.079	0.675	$\frac{-0.193}{7}$	35.62%
----	----	------	---	-------	-------	--------------------	---------------

Table A7: Forces on Rod in phase

In Phase Rod			
	x	y	z
spoke radius vector (in)	0	-4.592201188	-11.08655439
Force vector, relative to body weight	-0.15	0.25	1.5
Force vector (lbf)	-1.5	2.5	15
Moment vector (in-lb)	-41.16663185	-16.62983159	-6.888301783
Resultant Moment (in-lb)	44.92985175		
y (in)	0.32		
I (in ⁴)	0.008235497		
Bending stress on spoke (psi)	1745.802734		
Resultant force, compression only, rtbw	1.481490157		
compressive Force	14.81490157		
compressive stress (psi)	46.05204719		
	x	yz	magnitude
Resultant shear force, rtbw	-0.15	0.804995032	0.818851025
shear force			8.188510249
max shear stress (psi)	38.18091453		

Table A8 Forces on Rod out of phase

Out of Phase Rod			
	x	y	z
spoke radius vector (in)	0	-2.341083864	-11.76942336
Force vector, relative to body weight	-0.3	0.5	3
Force vector (lbf)	-3	5	30
Moment vector (in-lb)	-11.3853991	-35.30827009	-7.023251593
Resultant Moment (in-lb)	37.75748022		
y (in)	0.32		
I (in ⁴)	0.008235497		
Bending stress on spoke (psi)	1467.111723		
Resultant force, compression only, rtbw	3.039901002		
compressive Force	30.39901002		
compressive stress (psi)	94.49517012		
	x	yz	magnitude
Resultant shear force, rtbw	-0.3	1.075663606	1.116714912
shear force			11.16714912
max shear stress (psi)	52.06954049		

Table A9 Force in Tube in phase

Tube			
	x	y	z
spoke raduis vector (in)	0	-4.592201188	-11.08655439
Force vector,relative to body weight	-0.15	0.25	1.5
Force vector (lbf)	-1.5	2.5	15
Moment vector (in-lb)	-41.16663185	-16.62983159	-6.888301783
Resultant Moment (in-lb)	44.92985175		
y (in)	0.49		
I (in^4)	0.035384983		
Bending stress on spoke (psi)	622.174313		
Resultant force, compression only, rtbw	1.481490157		
compressive Force	14.81490157		
compressive stress (psi)	36.87765108		
	x	yz	maginitude
Resultant shear force, rtbw	-0.15	0.804995032	0.818851025
shear force			8.188510249
max shear stress (psi)	1317.068935		

Table A10 Force in Tube out of phase

Out of Phase Tube			
	x	y	z
spoke radius vector (in)	0	-2.34108386 4	-11.7694233 6
Force vector, relative to body weight	-0.3	0.5	3
Force vector (lbf)	-3	5	30
Moment vector (in-lb)	-11.3853991	-35.3082700 9	-7.02325159 3
Resultant Moment (in-lb)	37.7574802 2		
y (in)	0.49		
I (in ⁴)	0.03538498 3		
Bending stress on spoke (psi)	522.85359 07		
Resultant force, compression only, rtbw	3.03990100 2		
compressive Force	30.3990100 2		
compressive stress (psi)	75.670032 61		
	x	yz	magnitude
Resultant shear force, rtbw	-0.3	1.07566360 6	1.11671491 2
shear force			11.1671491 2
max shear stress (psi)	1796.1637 4		

Table A11 Factor of Safety and Fatigue Cycles

	Rod	Tube
Fatigue Factor of Safety (In Phase)	2.09839435	2.7814661
Fatigue Factor of Safety (Out of Phase)	2.497003151	2.039559375
Cycles (In Phase)	6.2807E+16	1.82769E+19
Cycles (Out of Phase)	2.08268E+18	1.40224E+16

Table A12: Sizings

Base Body Weight (lbf)	10
radius of rod (in)	0.32
outer radius of tube (in)	0.49
inner radius of tube (in)	0.335
cross sectional area, rod (in ²)	0.321699088
cross sectional area, tube (in ²)	0.401731161
length of rod	12

Table A13: Operational Range Test Results

Distance (feet)	Pass / Fail	Comments
10	Pass	
20	Pass	
30	Pass	
40	Pass	
50	Pass	Minimum Required Value
60	Pass	
70	Pass	
80	Pass	

90	Pass	
100	Pass	200% Minimum Required Value
110	Pass	
120	Pass	
130	Pass	
140	Pass	
150	Pass	300% Min. Required Value; Halted data collection

Table A14: Pugh Chart Matrix

Weight	Leg Design			
1-5	Selection Criteria	Rigid Feet	Spring Loaded Legs	Prosthetic Legs
4	Cost of Transport	2	3	4
5	Versatility	4	3	2
5	Manufacturing	3	4	1
3	Weight	4	4	3
4	Maintenance	3	4	2
2	Size	4	4	4
3	Simplicity	3	3	2
	Total	84	92	62

Table A15: Speed Test Results

T r i a l Number	Distance (feet)	T i m e (sec)	Experimental Velocity (ft/s)	Experimental Velocity (MPH)
1	6	1.14	5.263	3.589
2	6	1.07	5.607	3.823
3	6	1.25	4.800	3.273
4	6	2.63	2.281	1.555
5	6	1.02	5.882	4.011
6	6	2.10	2.857	1.948
7	6	0.90	6.667	4.545
8	6	1.05	5.714	3.896

9	6	1.04	5.769	3.934
10	6	1.4	4.286	2.922
11	6	1.41	4.255	2.901
12	6	1.62	3.704	2.525

Table A16: 3-D Part Dimension Test Results

Leg #	Tube Thickness (in)	Tube O.D.(in)	Tube Length (in)	Rod O.D (in)	Rod Length (in)
1	0.065	0.801	3.613	0.640	7.501
2	0.066	0.803	3.611	0.640	7.504
3	0.064	0.799	3.615	0.640	7.502
4	0.061	0.8	3.612	0.640	7.498
5	0.066	0.798	3.611	0.640	7.503
6	0.061	0.801	3.61	0.641	7.499
7	0.061	0.803	3.611	0.640	7.501
8	0.063	0.801	3.615	0.639	7.504
9	0.067	0.805	3.614	0.638	7.501
10	0.063	0.801	3.615	0.640	7.504
11	0.063	0.799	3.61	0.640	7.504
12	0.065	0.801	3.613	0.638	7.498
13	0.065	0.800	3.608	0.640	7.500
14	0.065	0.800	3.613	0.639	7.503
15	0.065	0.798	3.613	0.639	7.498
16	0.065	0.796	3.610	0.639	7.498
AVG	0.064	0.800	3.612	0.640	7.50

<u>Expected Measurements</u>
Tube Thickness: 0.065"
Tube O.D.: 0.800"
Tube Length: 3.61"
Rod O.D.: 0.640"
Rod Length: 7.5"

Figure A11: Expected 3-D Part Dimensions

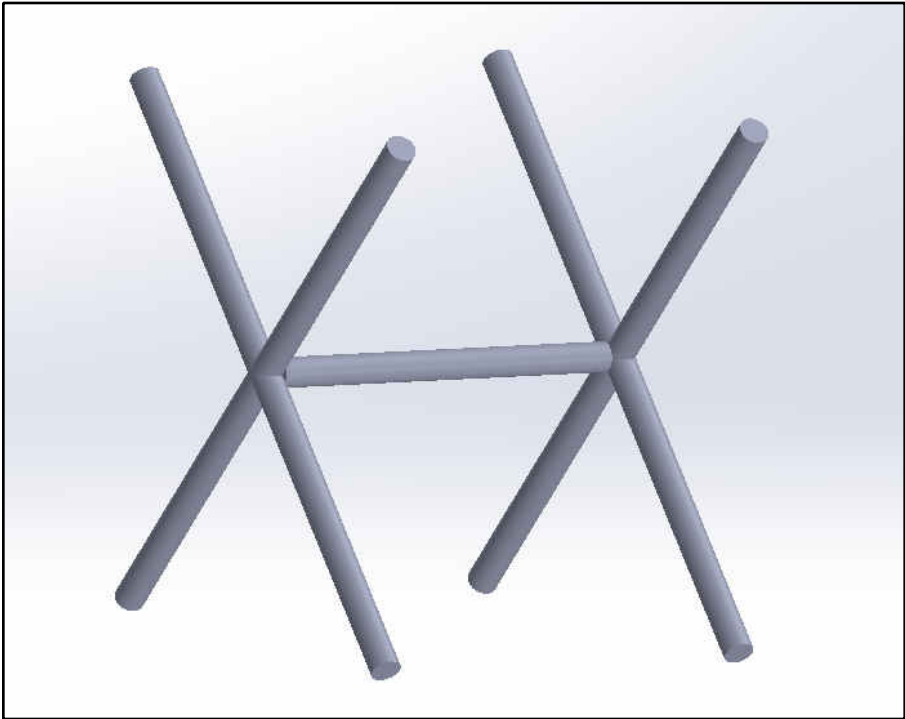


Figure A12: Approximate Shape

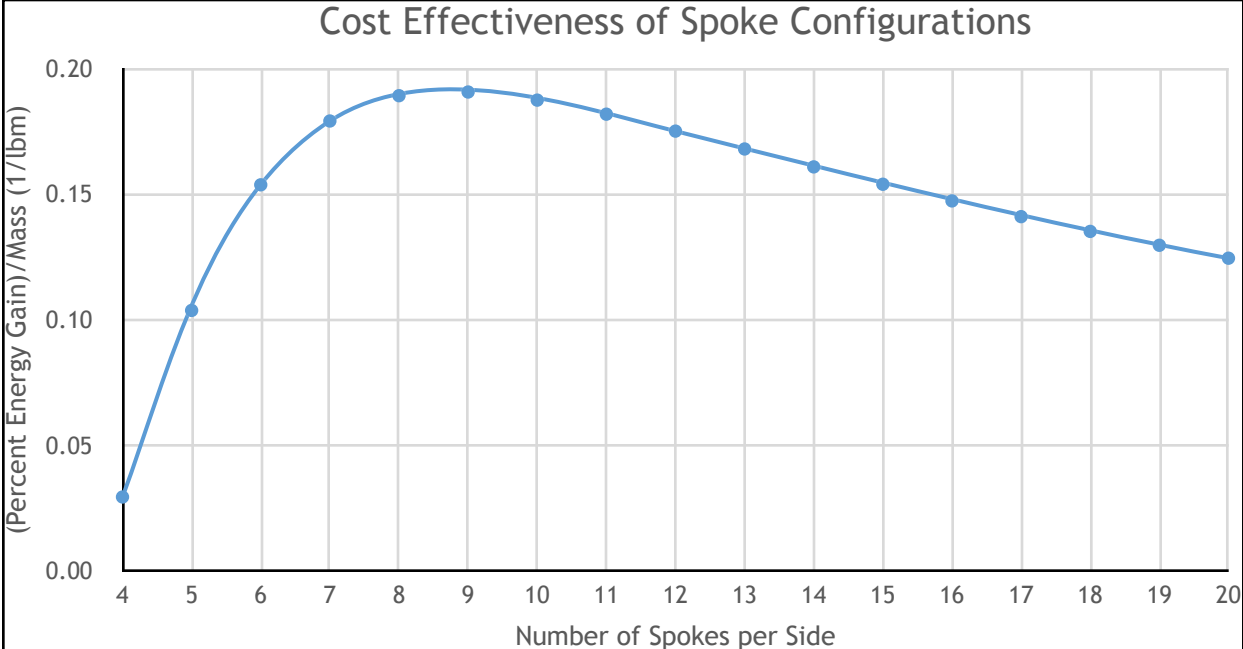


Figure A13: Cost Effectiveness of Spoke Configurations

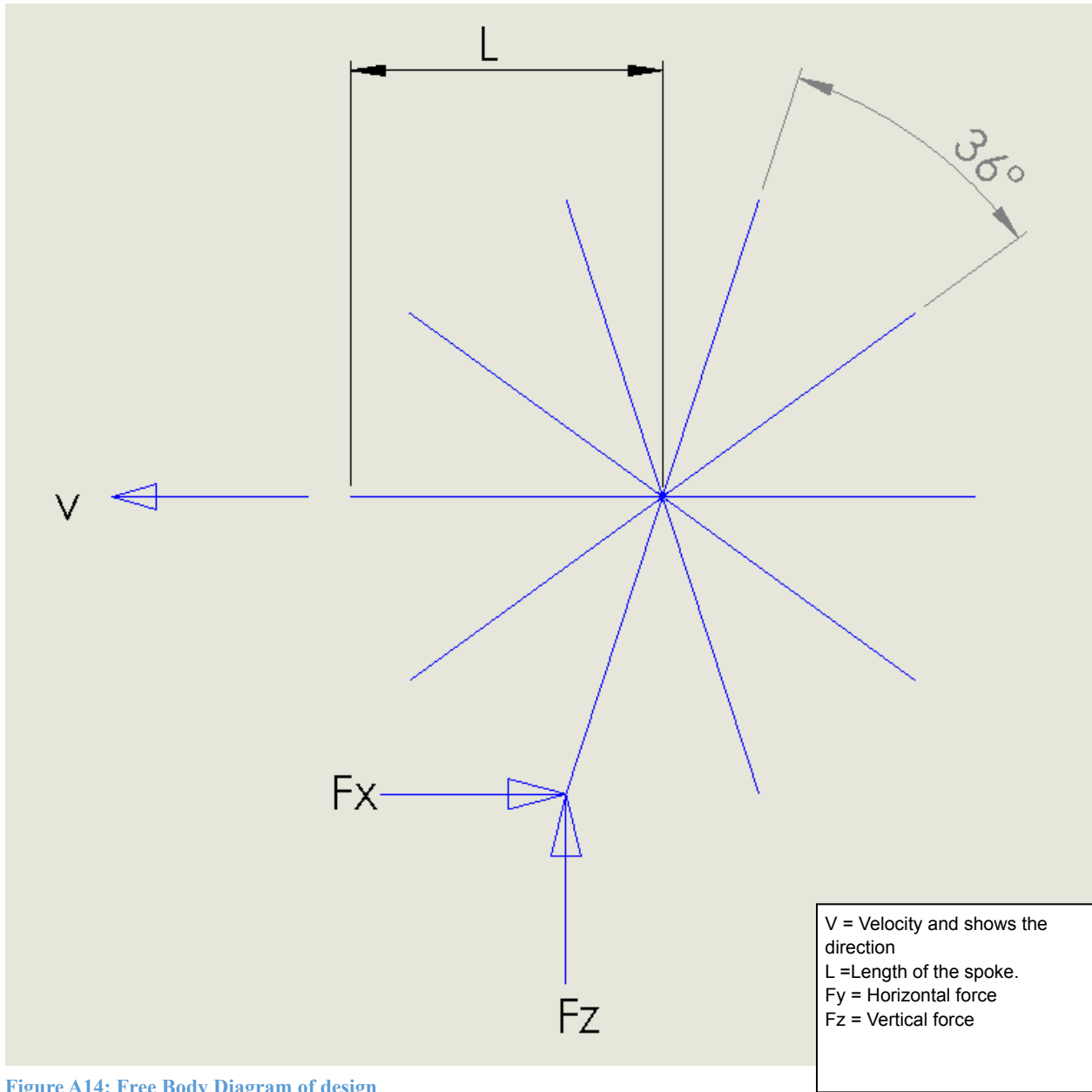


Figure A14: Free Body Diagram of design

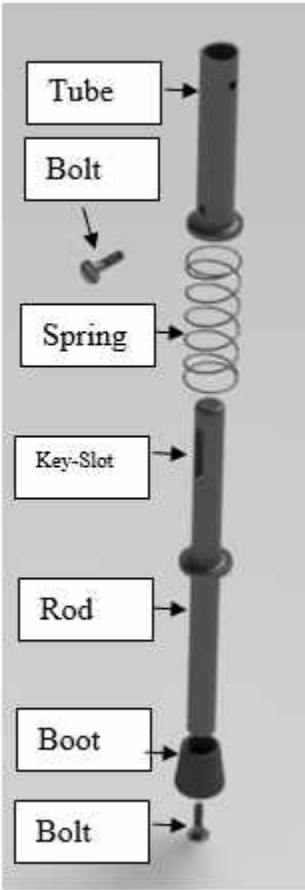


Figure A15: Exploded Leg assembly

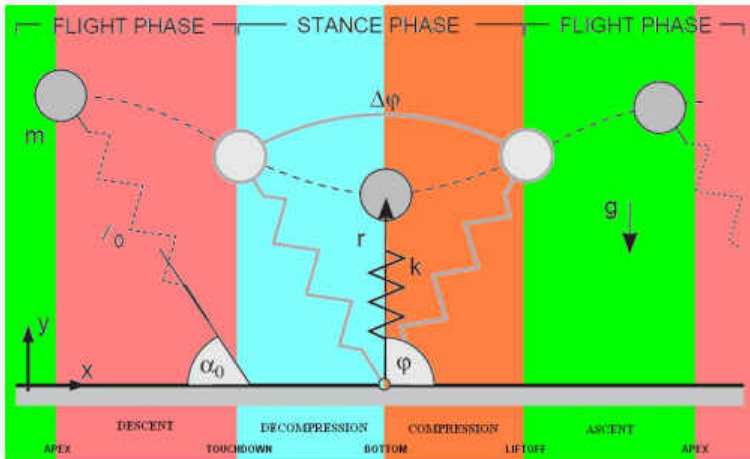


Figure A16: Spring Loaded Inverted Pendulum (SLIP) System

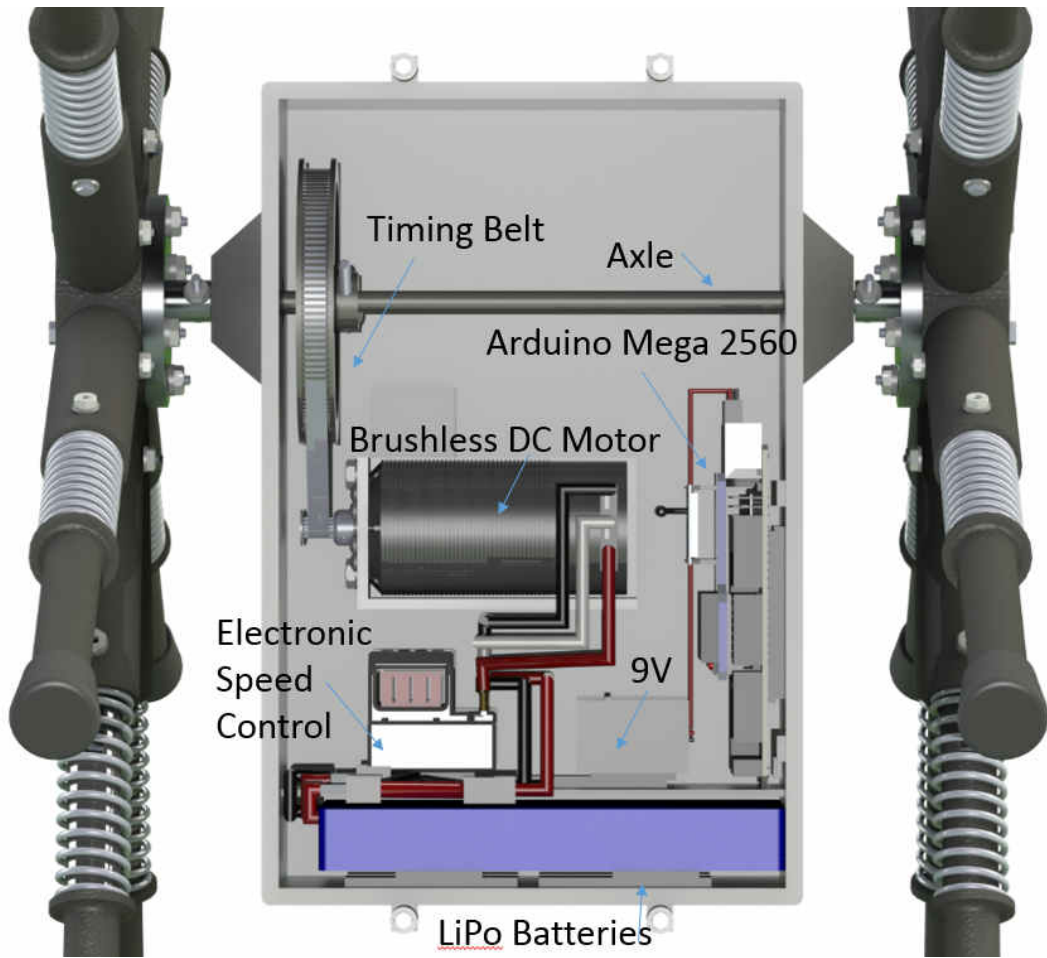
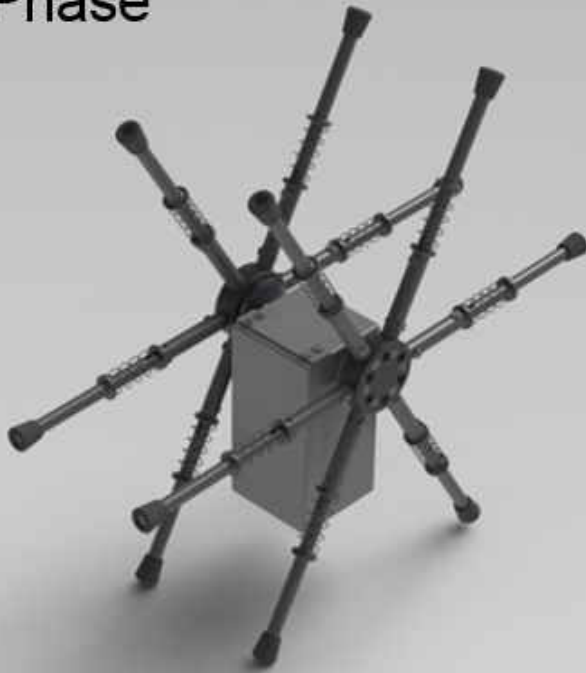


Figure A17: Case Layout

In Phase



Anti-Phase

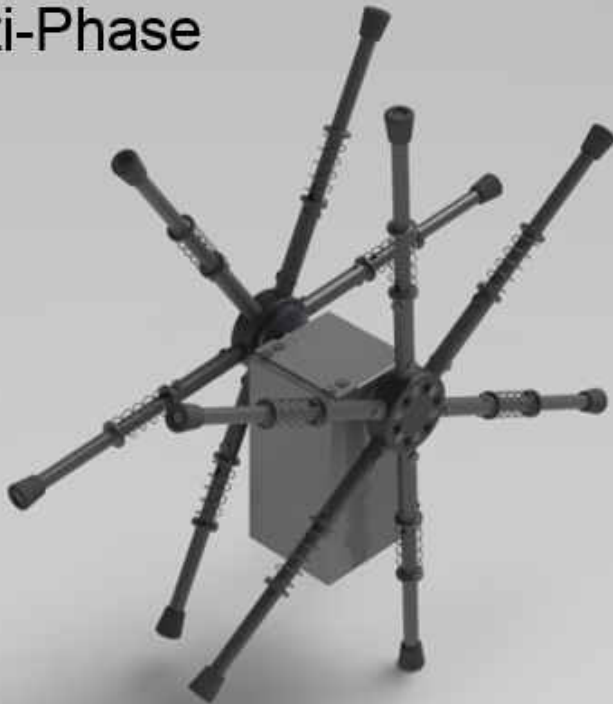


Figure A18: Robot In-Phase and Anti-Phase

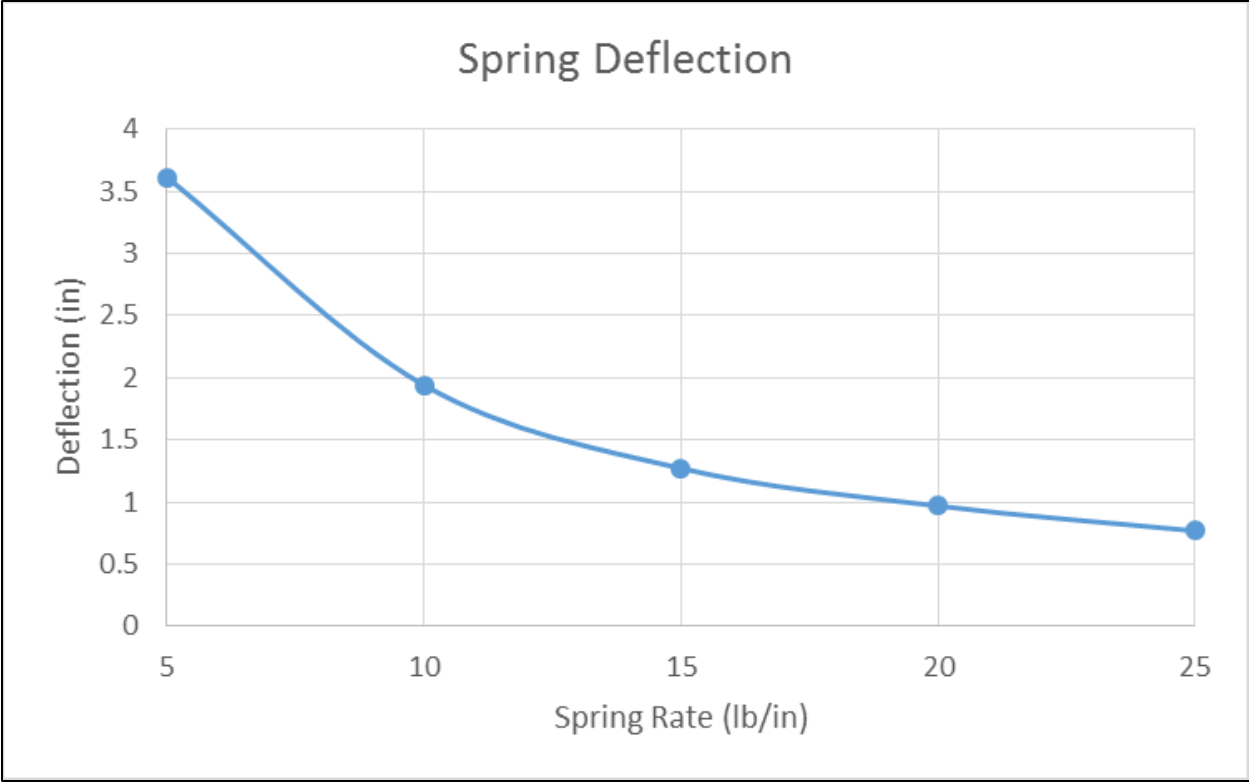


Figure A19: Deflection of Spring at 4 MPH

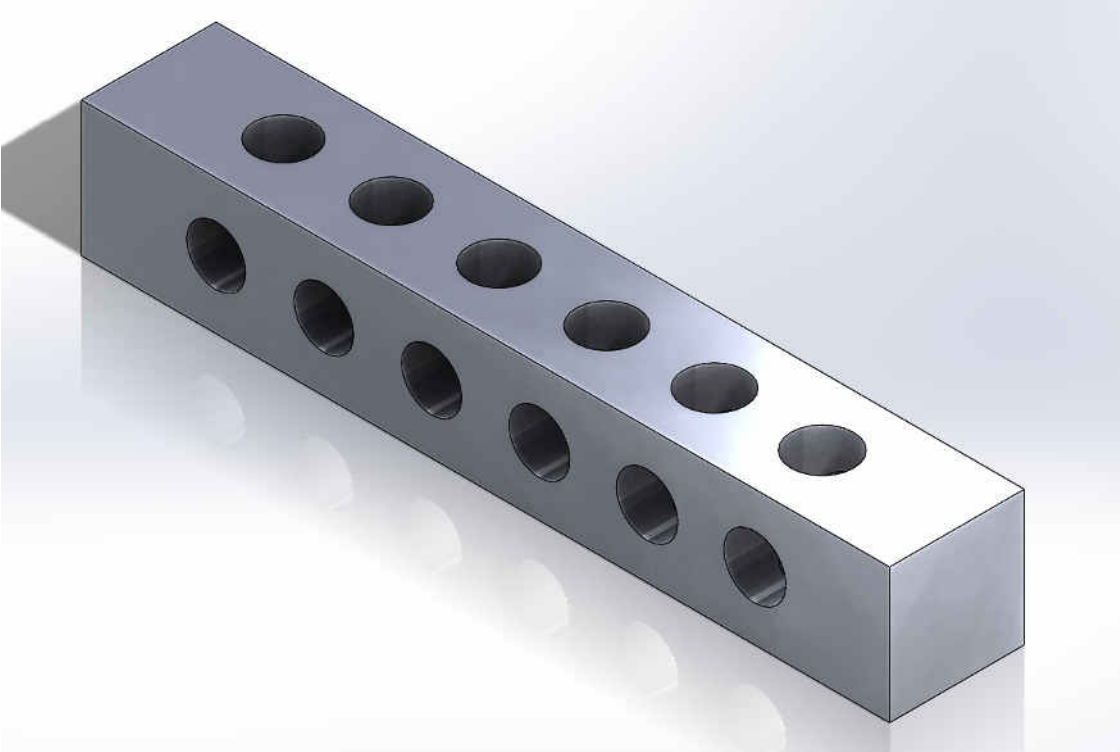


Figure A20: Bearing Test Fixture

15. Appendix B

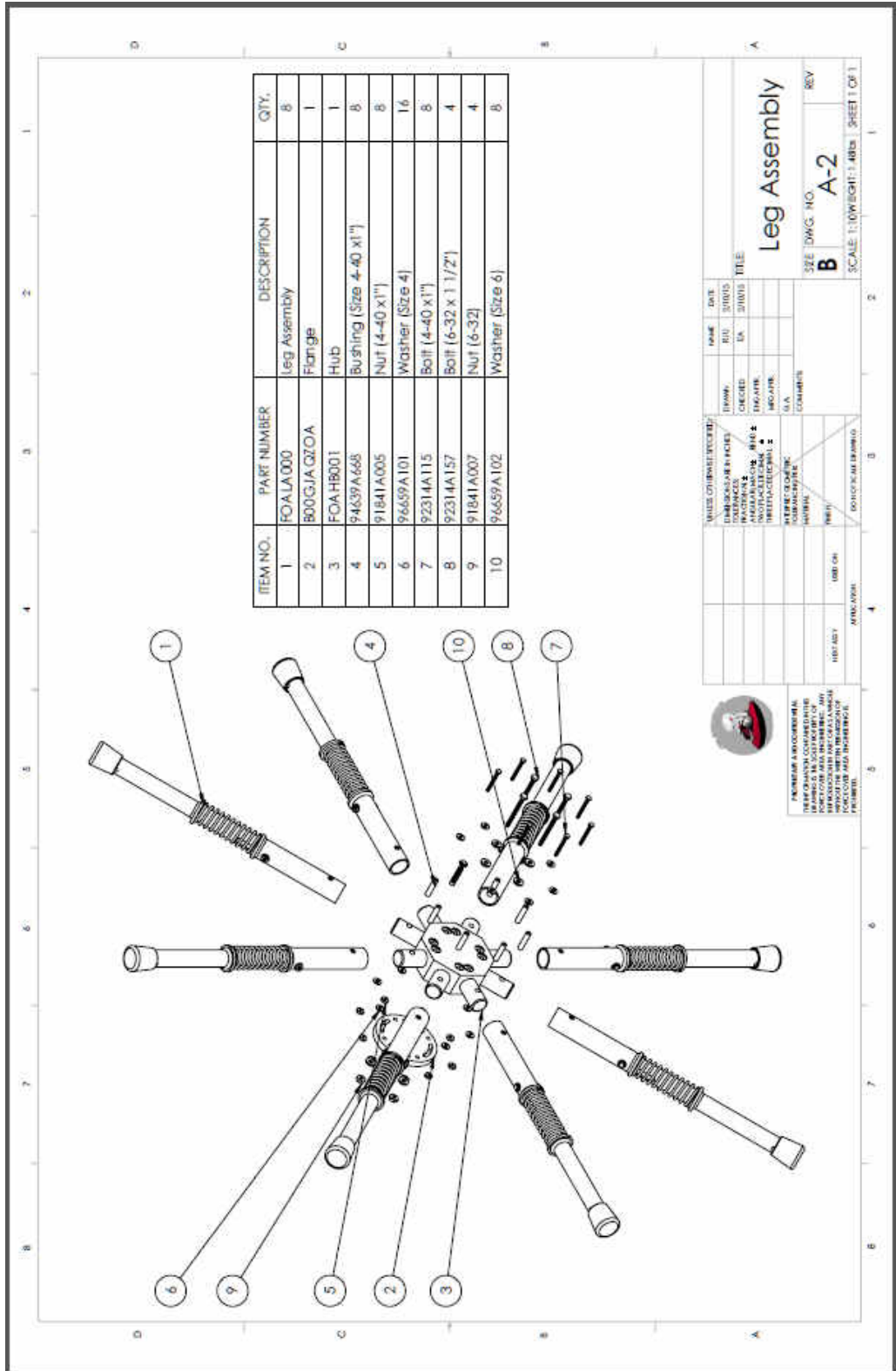


Figure B21: Leg Assembly

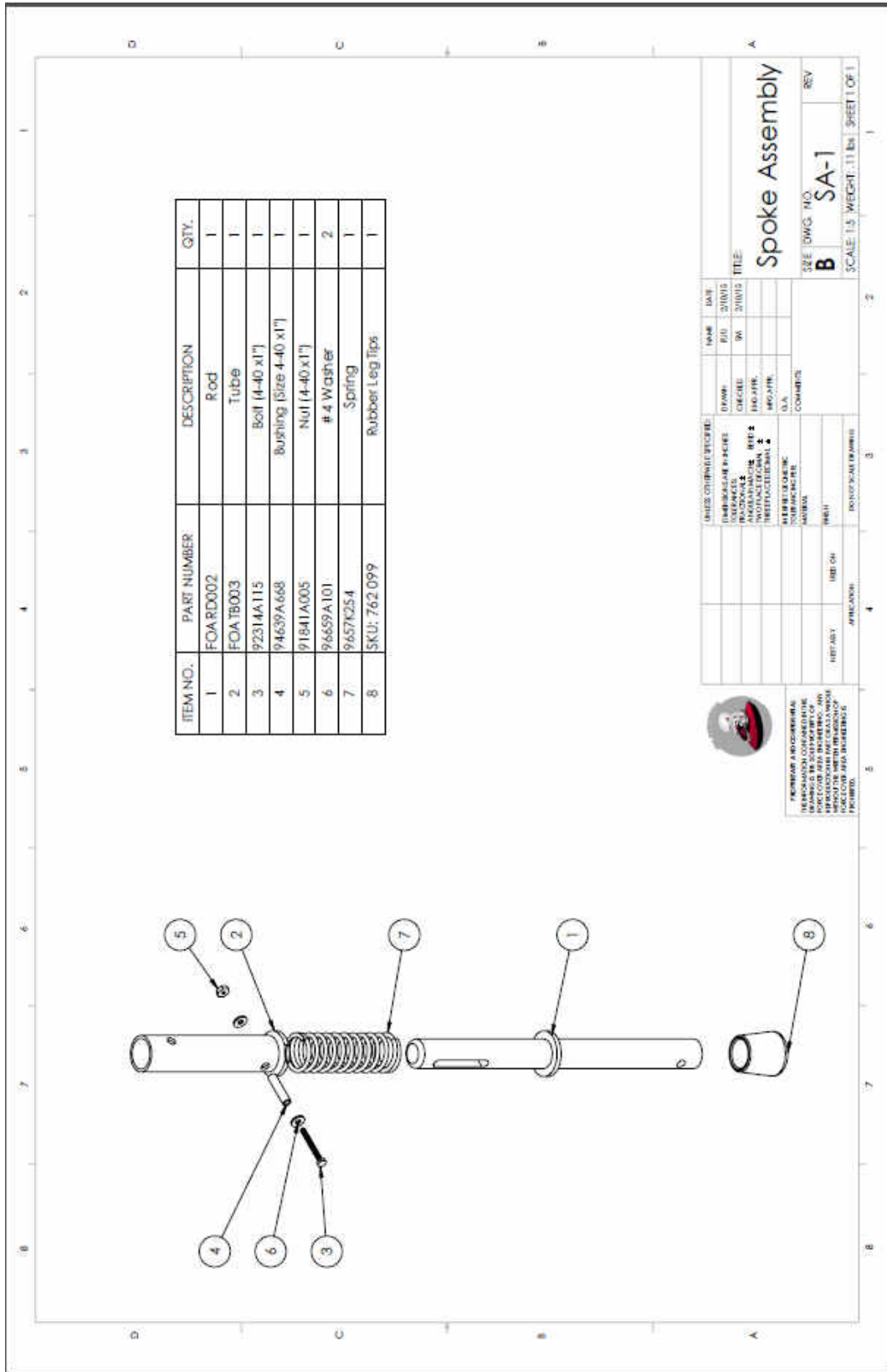


Figure B22: Spoke Assembly

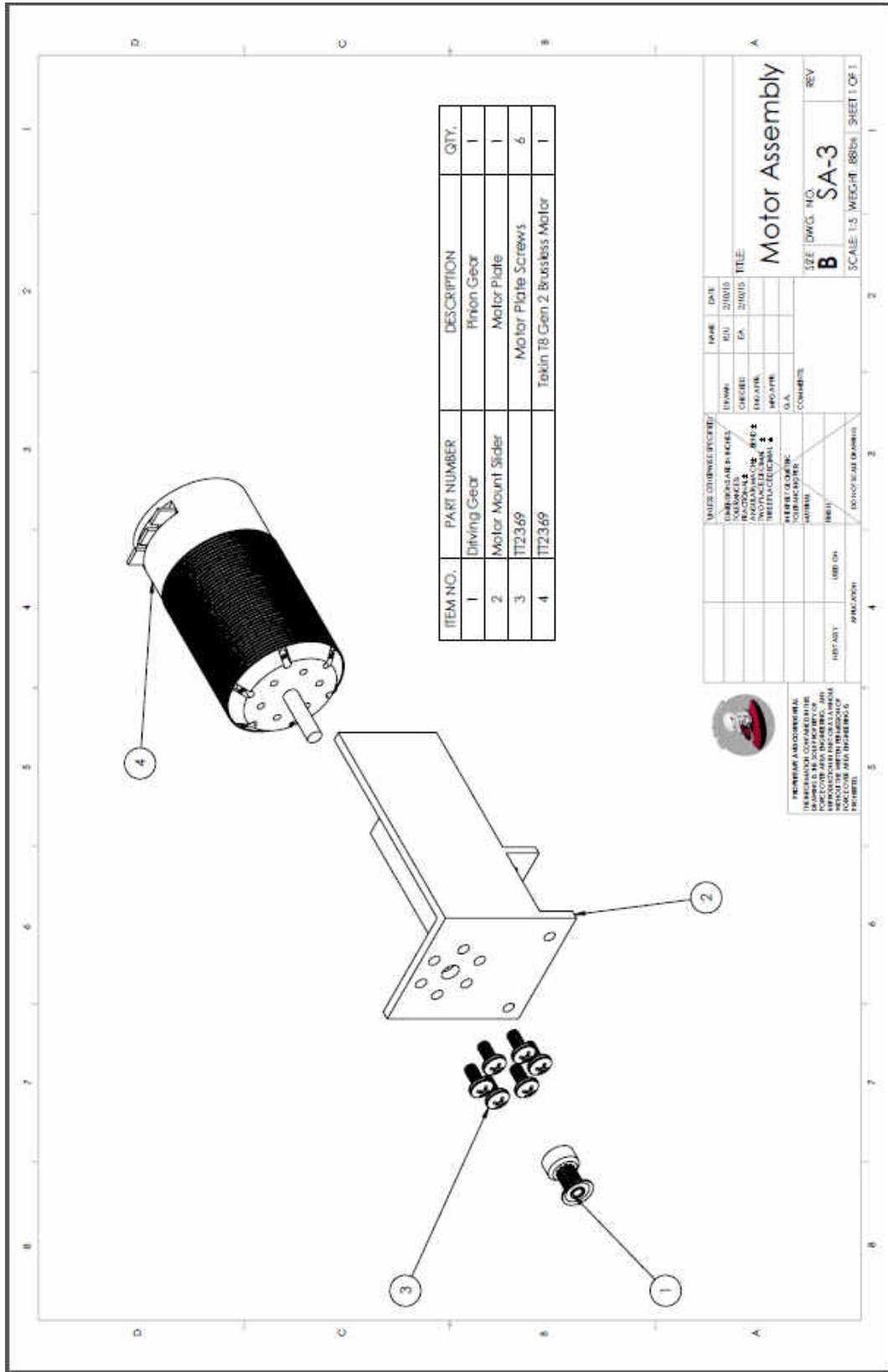


Figure B24: Motor Assembly

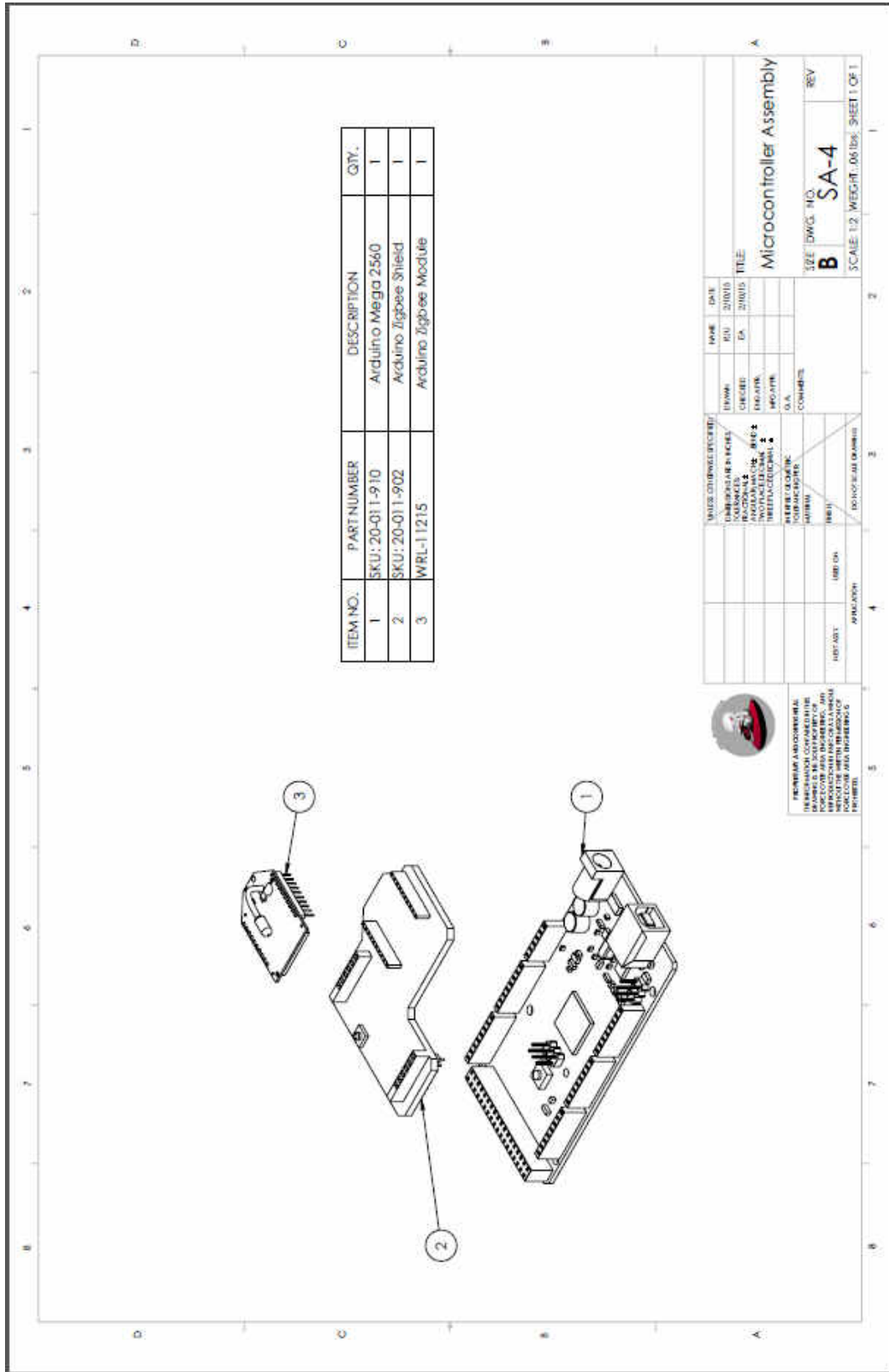


Figure B25: Microcontroller Assembly

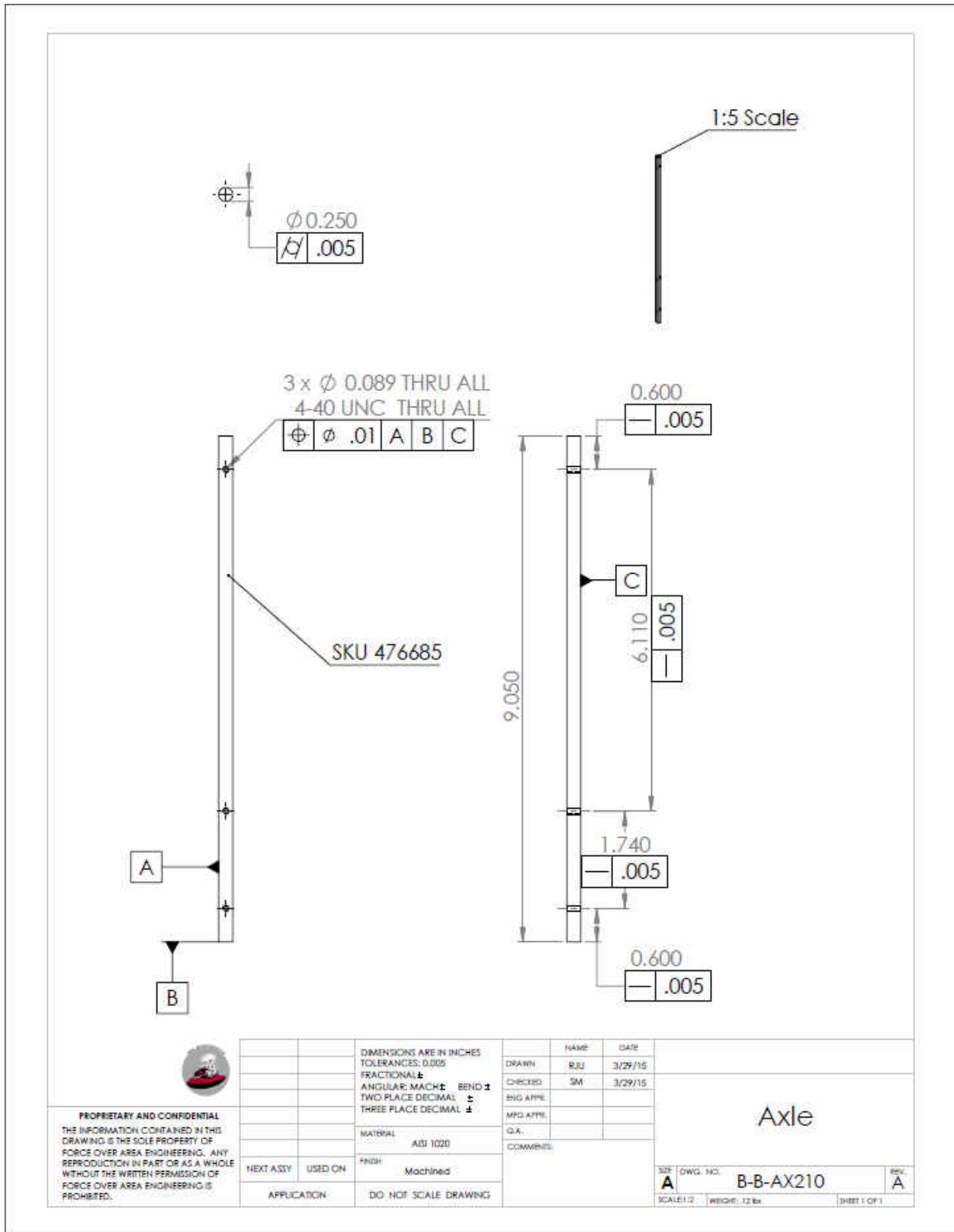


Figure B26: Axle

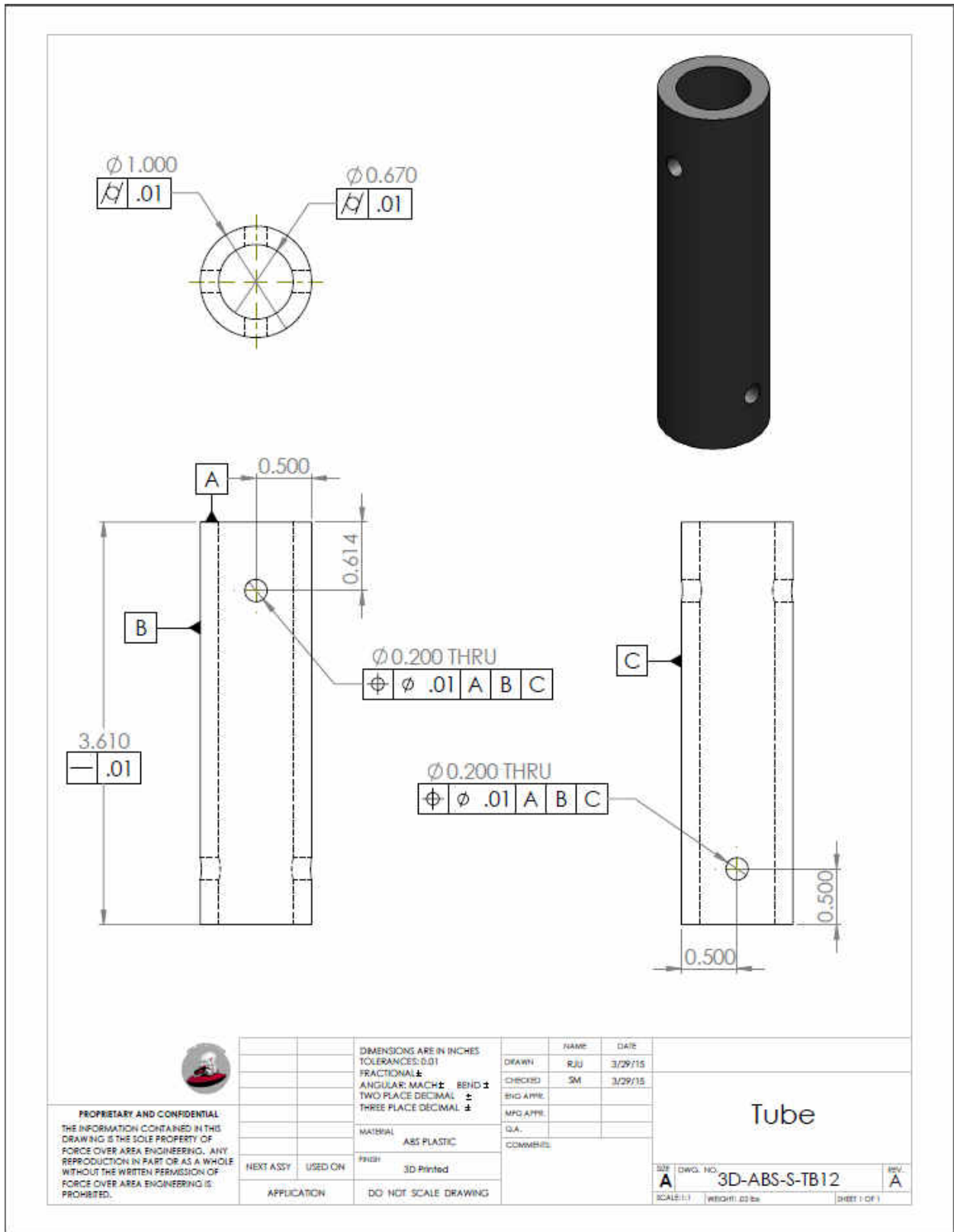


Figure B27: Tube

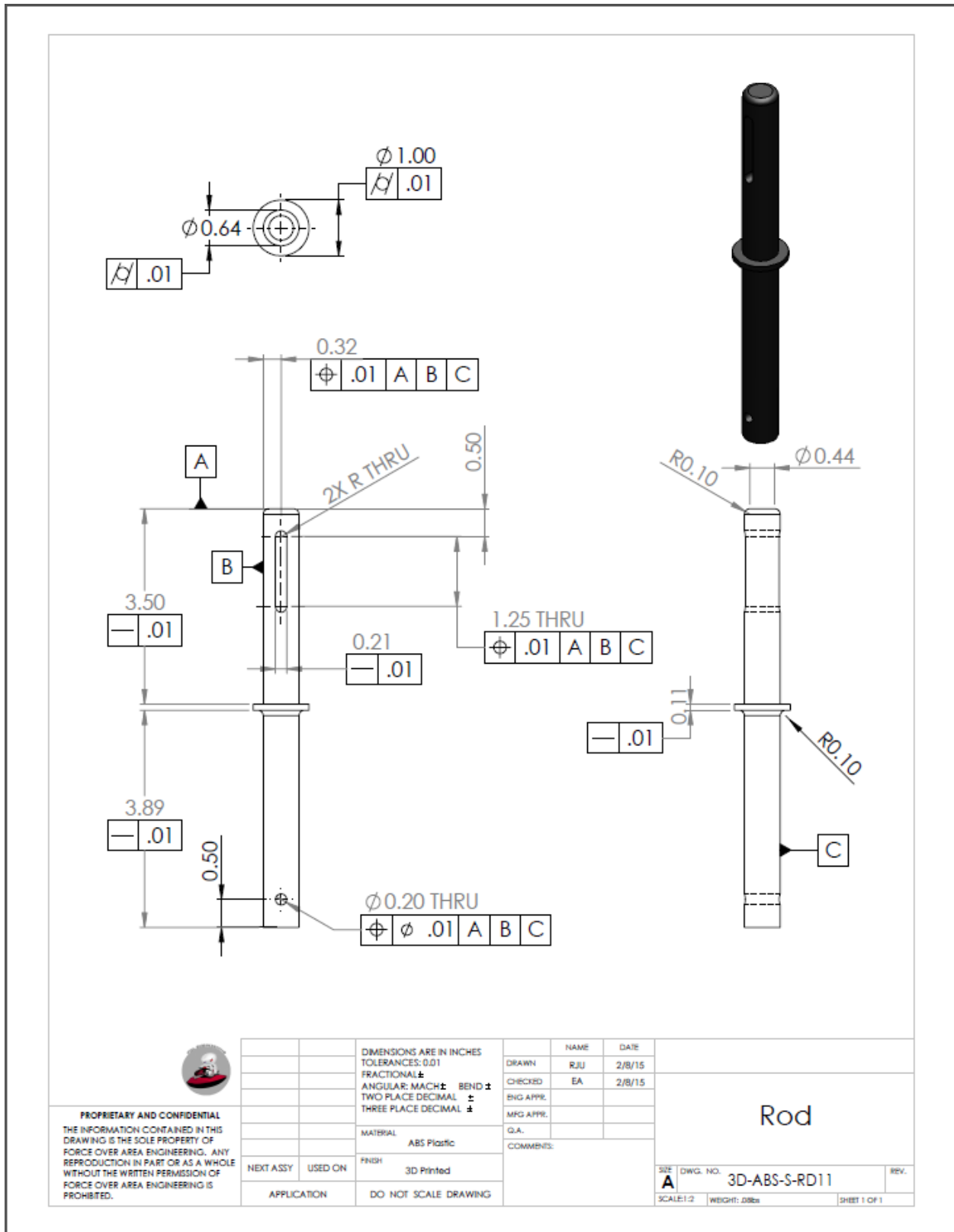


Figure B28: Rod

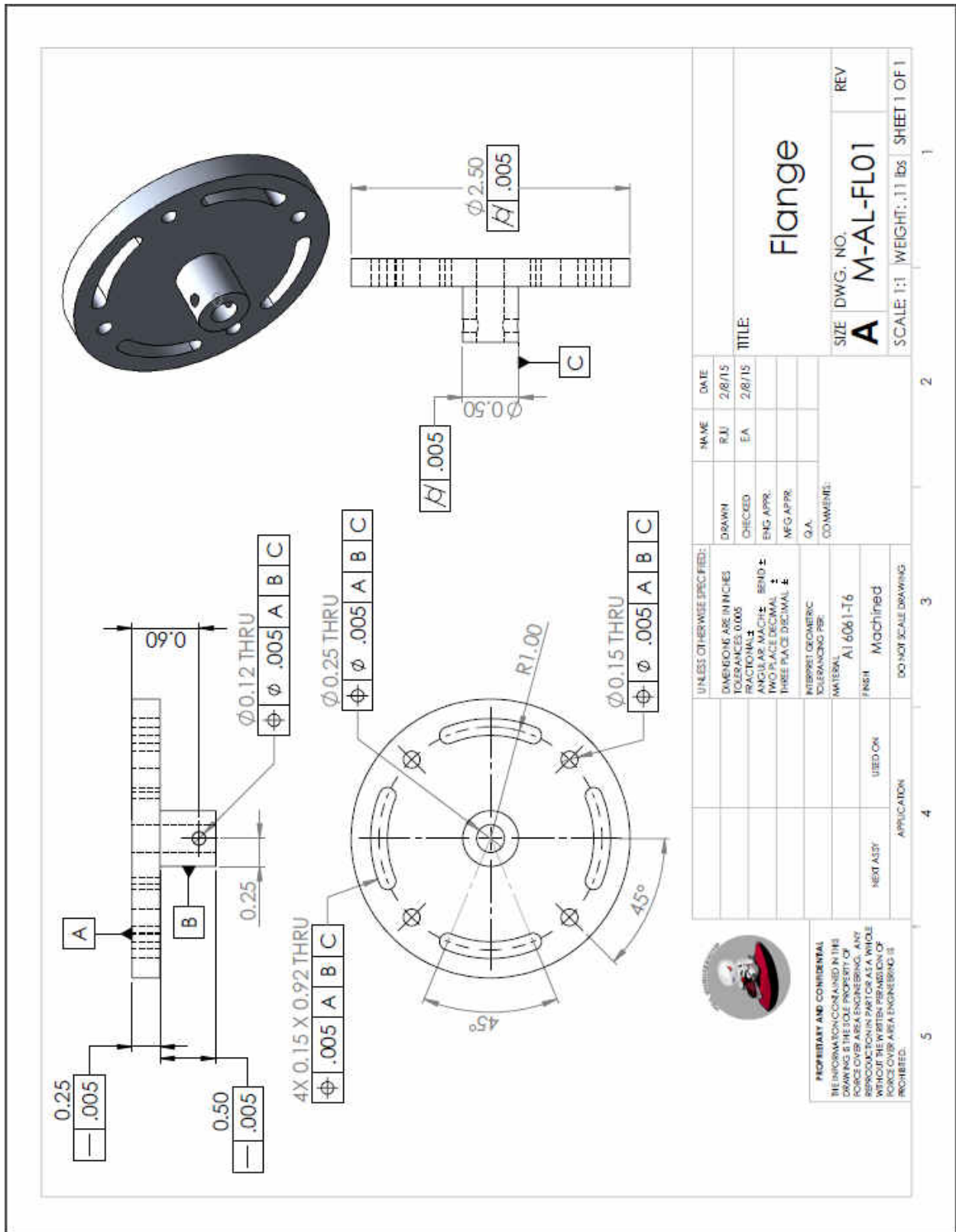


Figure B29: Flange

UNLESS OTHERWISE SPECIFIED:		NAME	DATE
DIMENSIONS ARE IN INCHES	TOLERANCES 0.005	RJ	28/15
FRACTIONAL ±	DECIMAL ±	EA	28/15
ANGULAR MACH ±	SEMI ±		
TWO PLACE DECIMAL ±	THREE PLACE DECIMAL ±		
INTERPRET DIMETRIC TOLERANCING PER:	Q.A.		
MATERIAL	COMMENTS:		
A1 6061-T6			
FINISH			
Machined			
NEET ASSY	USED OK		
APPLICATION	DO NOT SCALE DRAWING		

UNLESS OTHERWISE SPECIFIED:		NAME	DATE
TITLE: Flange			
SIZE	DWG. NO.	REV	
A	M-AL-FLO1		
SCALE: 1:1	WEIGHT: .11 lbs	SHEET 1 OF 1	1

5 4 3 2 1

PROPRIETARY AND CONFIDENTIAL
 THE INFORMATION CONTAINED IN THIS
 DRAWING IS THE SOLE PROPERTY OF
 FORCE OVER AREA ENGINEERING. ANY
 REPRODUCTION IN PART OR AS A WHOLE
 WITHOUT THE WRITTEN PERMISSION OF
 FORCE OVER AREA ENGINEERING IS
 PROHIBITED.

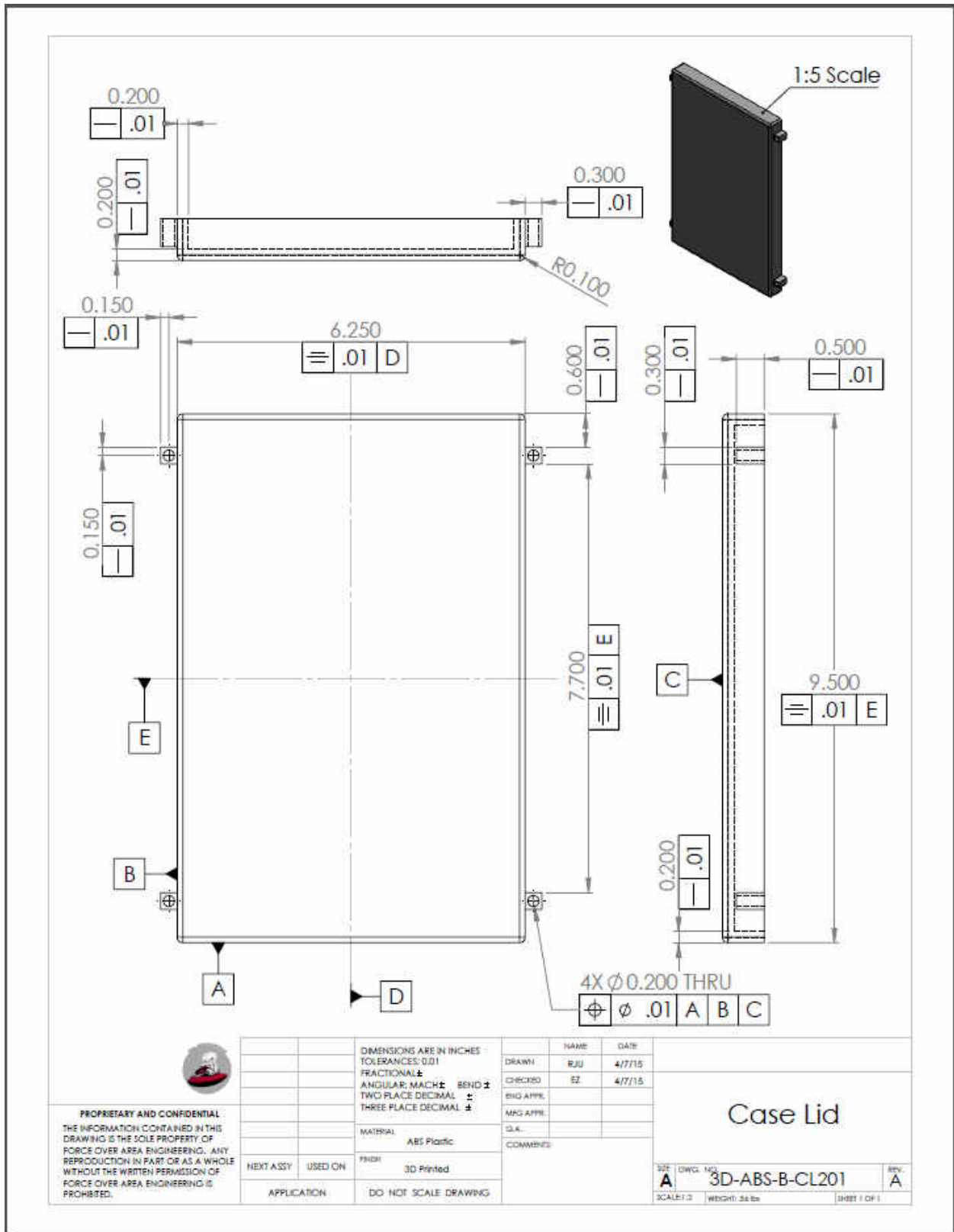


Figure B31: Case Lid

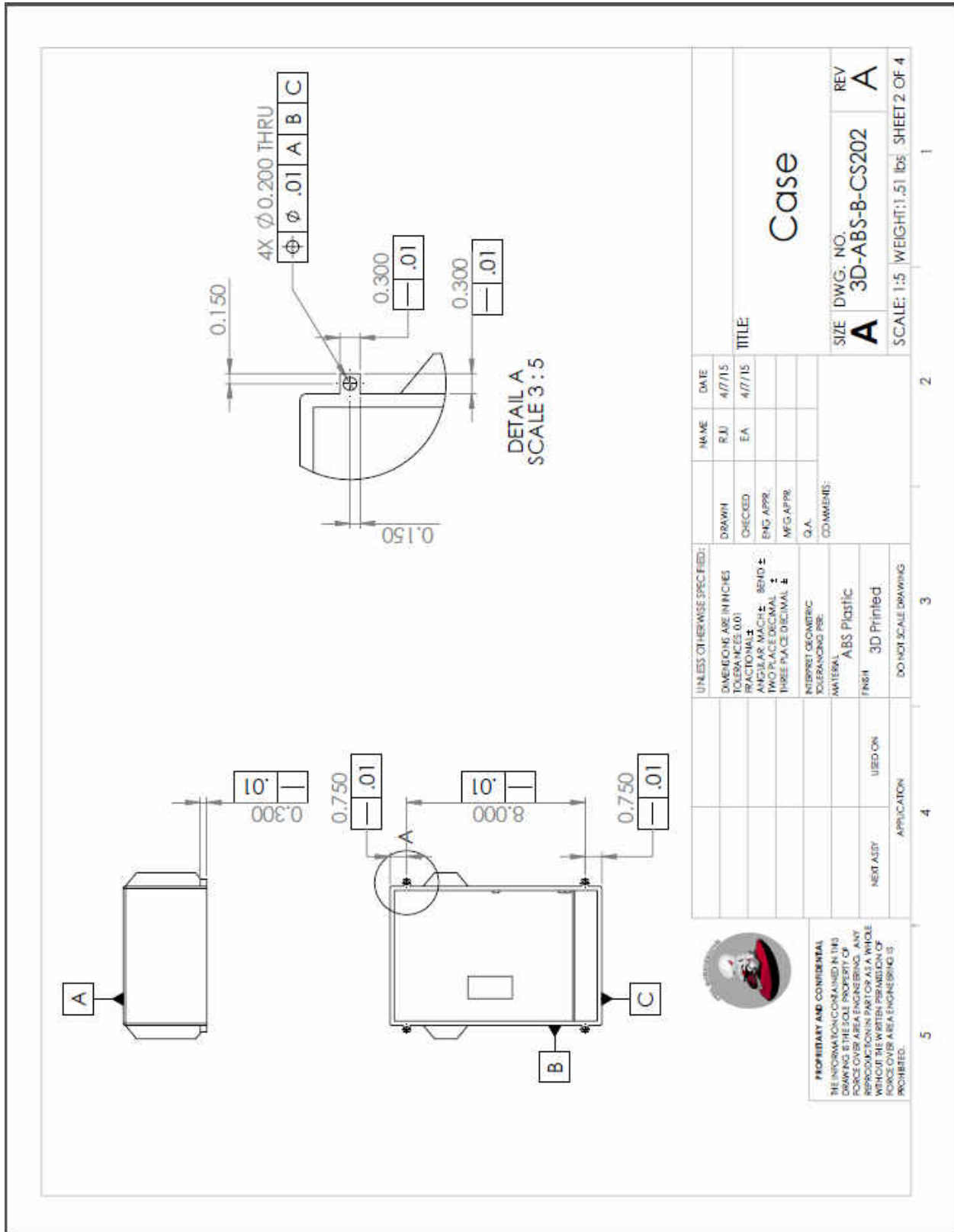


Figure B33 Case 2

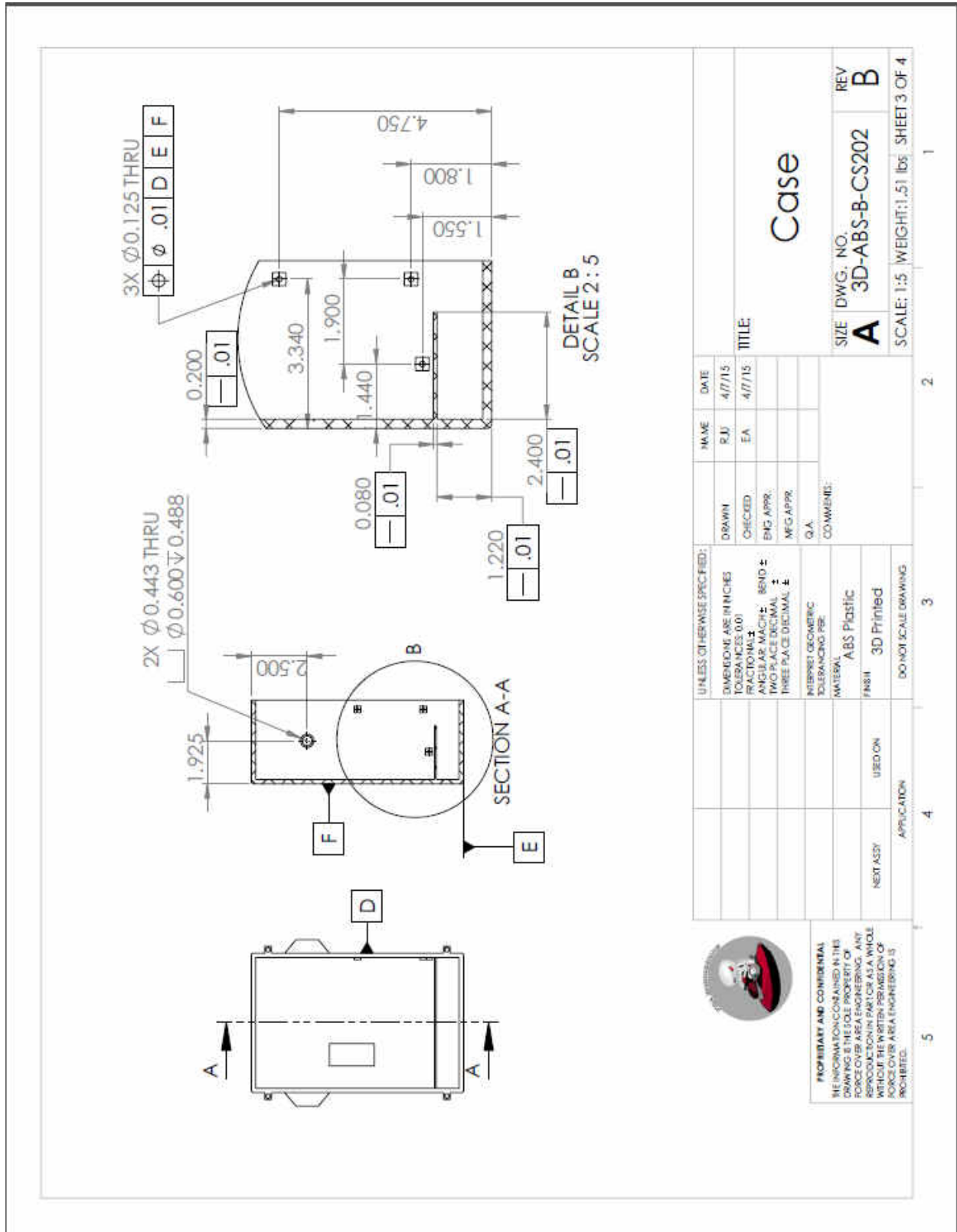


Figure B34: Case 3

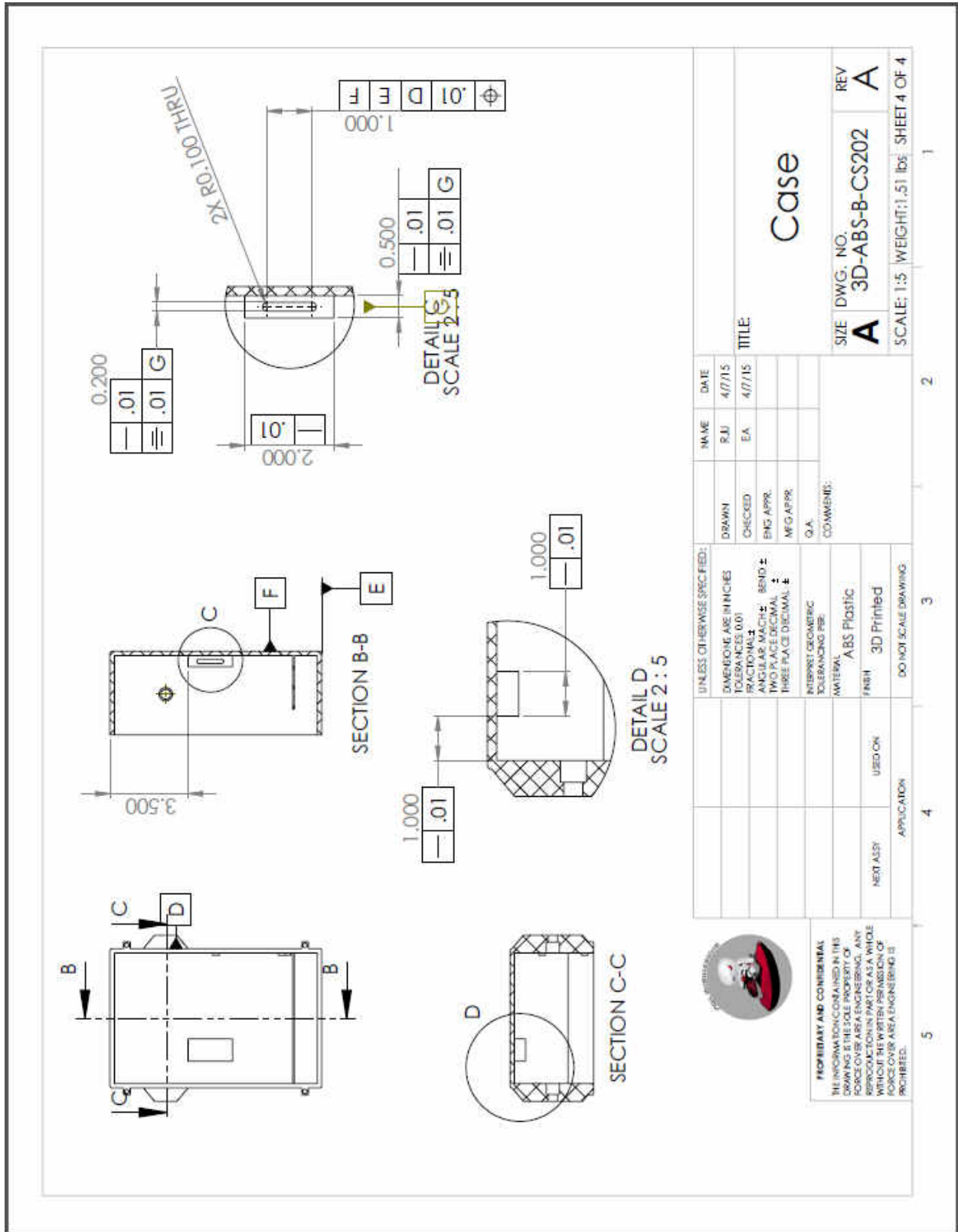


Figure B35: Case 4

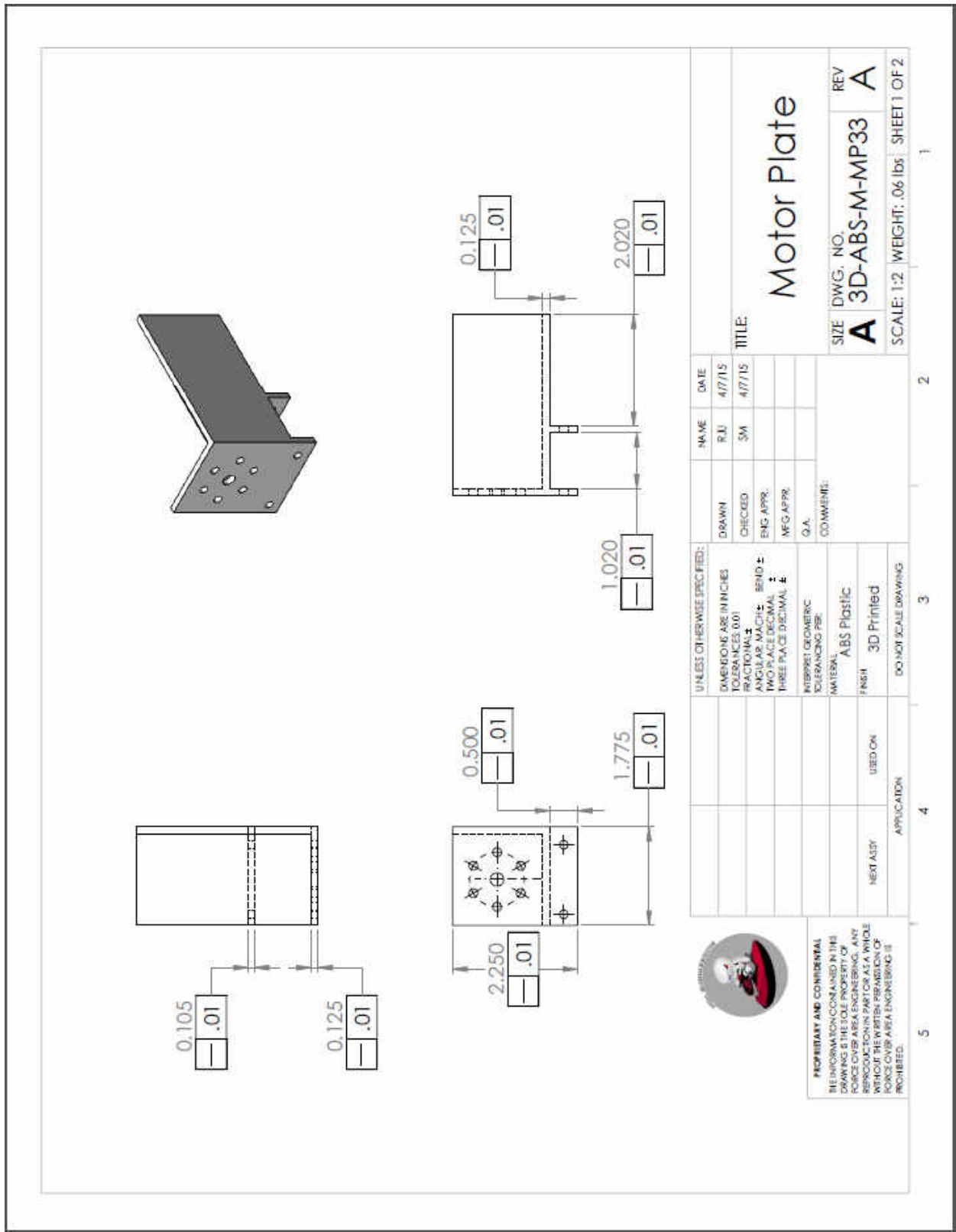


Figure B36: Motor Plate 1

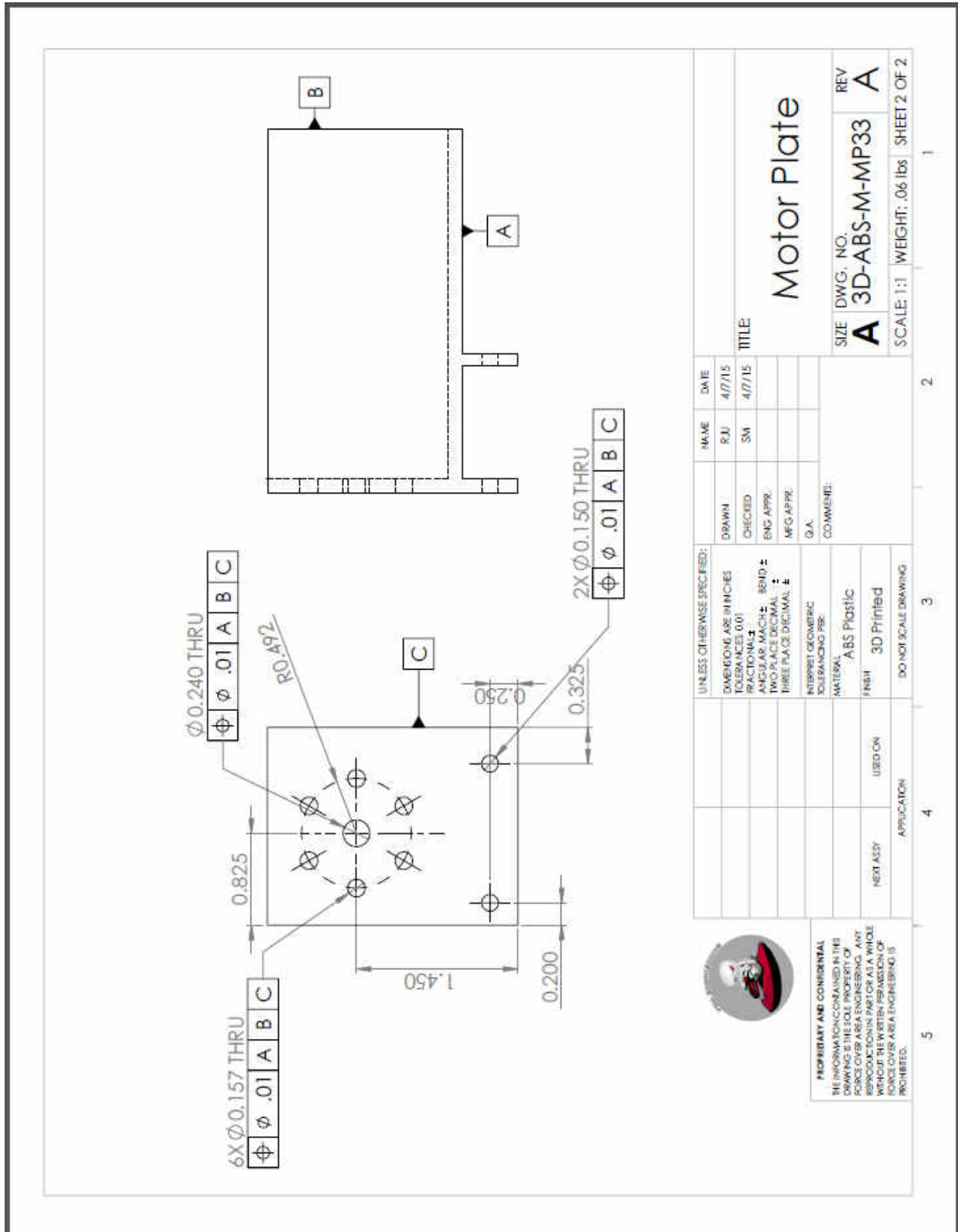


Figure B37: Motor Plate 2

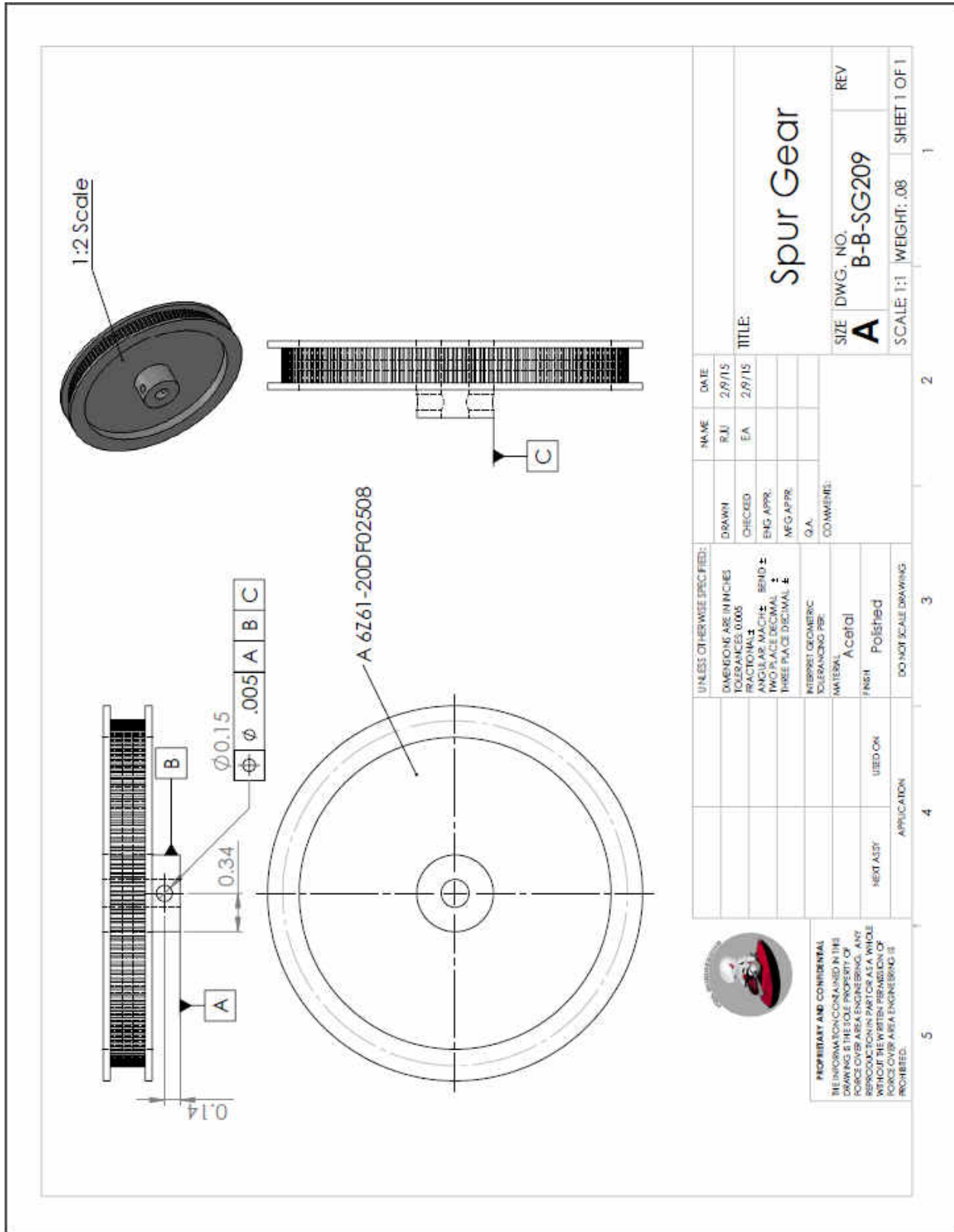


Figure B38: Spur Gear